

DIRK OLBERS (dolbers@awi-bremerhaven.de)

## 58.1 Introduction

The ocean is turbulent at all scales but the nature of turbulence depends critically on the scale under consideration and thus turbulence in the ocean comes in many different species. In the present chapter we are dealing with planetary-scale currents and the turbulence field interacting with these. The relevant eddy scales are in the so-called mesoscale range; depending on site – i.e. stratification and Coriolis parameter – this range is roughly from 10 to 100 km. The intrinsic scale arising from the dynamic equations is the baroclinic Rossby radius  $Nh/f$ , where  $N$  is the buoyancy frequency,  $f$  the Coriolis frequency, and  $h$  the ocean depth. The Rossby radius is the preferred scale of baroclinic instability of large-scale currents with vertical shear (see e.g. Pedlosky [1987]). If the current is unstable (barotropic instability may combine with the baroclinic instability in a mixed process), eddies with scales of a few Rossby radii arise, drawing energy from the potential energy of the shear flow. Via Reynolds stresses and – as we shall outline in this chapter – via eddy-induced interfacial form stress, the turbulent field interacts with the mean flow, reshaping it by feeding eddy kinetic energy into mean kinetic energy, whereby the system may come to an equilibrated state, described by the Lorenz energy cycle for zonal flow (Lorenz 1967).

A frequently studied object in this area – since pre-computer times a paradigm of atmospheric research – is the large-scale geostrophic, stratified zonal current in the zonally periodic domain. The model concept was employed for analytical investigations of baroclinic instability of zonal flows (Charney [1947] and Eady [1949]; see Pedlosky [1987]) and served later in numerous studies of geophysical fluid dynamics, such as the development of parameterization concepts for the turbulent transports achieved by mesoscale eddies (e.g. Green, [1970]; Stone, 1972; Held, 1978; Held and Larichev, 1996), turbulent shear flow on the  $\beta$ -plane (e.g. McWilliams *et al.*, 1978; McWilliams and Chow, 1981; Vallis, 1988; Wolff *et al.*, 1991), and homogeneous  $\beta$ -plane turbulence (e.g. Larichev and Held, 1995; Pavan and Held, 1996).

The most important examples of zonal mean flow in the atmospheric circulation are found in the westerly jet streams in both hemispheres, but there is only one example of a zonally unrestricted current in the world ocean, namely

the Antarctic Circumpolar Current (ACC). The uniqueness of this current is manifested by many outstanding properties: it is the only important conduit linking the Atlantic, Pacific, and Indian Oceans; with its length of roughly 20 000 km it is the longest continuous ocean current; with a transport in the range<sup>1</sup> 130 Sv (through Drake Passage, Whitworth [1983]) to 150 Sv (between Tasmania and Antarctica, Rintoul and Sokolov [2001]) it is the largest of the world ocean's current systems; its vertical structure is baroclinic but it does not exhibit significant inversions of the velocity (e.g. Olbers and Wenzel, 1989) and direction (e.g. Killworth, 1992) with depth as other large currents do; though eddy activity is present in all large-scale currents in the world ocean and though marine topography plays a steering role in most of these currents, these two features are responsible for balance properties of heat and momentum that are unique to the ACC. The last-mentioned properties are the concern of the present chapter. Further observational and theoretical concepts and results can be found in the recent reviews of Olbers (1998) and Rintoul *et al.* (2001).

Eddies are defined here as features in the difference field of the instantaneous and the time-mean circulation. These will be called “transient eddies.” There is another class of eddies in geophysical current that arise if the time-mean current is not zonal but undulating due to non-zonal forcing or topography (both conditions are found in the ACC). It has become customary to call the difference field of the time mean and the time-plus-zonal mean the “standing eddies.”

Most of the ingredients of the physics of zonal currents used here can be elucidated by reference to a simple conceptual model. Consider a zonally unbounded strip of ocean with the ACC imbedded and split the water column into three layers (which may be stratified) separated by isopycnals. The upper layer of thickness  $\eta_1$  includes the Ekman layer, the intermediate layer with base at  $z = -\eta_2$  lies above the highest topography in the Drake Passage belt (the range of latitudes running through Drake Passage), and the lower one reaches from  $z = -\eta_2$  to the ocean bottom at  $z = -h$ . On writing the depth and zonally integrated northward volume flux in each layer as  $V_i$ ,  $i = 1, 2, 3$ , the

<sup>1</sup> 1 Sv =  $10^6 \text{ m}^3 \text{ s}^{-1}$ .

time and zonally averaged balance of zonal momentum reads<sup>2</sup>

$$\begin{aligned} -f\bar{V}_1 &= -\overline{\eta_1^* p_{1x}^*} + \tau_0 - \tau_1 - R_1, \\ -f\bar{V}_2 &= \overline{\eta_1^* p_{1x}^*} - \overline{\eta_2^* p_{2x}^*} + \tau_1 - \tau_2 - R_2, \\ -f\bar{V}_3 &= \overline{\eta_2^* p_{2x}^*} - \overline{h p_{bx}} + \tau_2 - \tau_b - R_3, \end{aligned} \quad (58.1)$$

where  $p_i$  are the pressures in the respective layers,  $p_3 = p_b$  is the bottom pressure, the overbar denotes the time- and-zonal mean, the star denotes the deviation from this average (the starred quantities thus include transient and standing eddies),  $\tau_0$  is the zonal wind stress,  $\tau_i$  are the frictional stresses at interfaces,  $\tau_3 = \tau_b$  is the frictional bottom stress, and  $R_i$  are the divergences of appropriate lateral Reynolds stresses. The meridional circulation is characterized by the pattern of meridional transports  $\bar{V}_i$ , which, in this isopycnal framework, are of Lagrangian quality. The Eulerian parts of  $\bar{V}_i$  consist of the wind-driven component  $-\tau_0/f$  (the Ekman transport) in the top layer and a geostrophic component in the bottom layer, which is associated with the bottom form stress  $\overline{h p_{bx}}$ . Since  $\sum_i \bar{V}_i = 0$  by mass balance and assuming that  $R_i$  and the bottom frictional stress  $\tau_b$  can be neglected, these Eulerian parts of the meridional circulation must balance, and the same argument states that the overall balance of zonal momentum is that between the applied wind stress and the bottom form stress,

$$\tau_0 \simeq \overline{h p_{bx}}. \quad (58.2)$$

This balance has been confirmed for most of the numerical models which include the opposition of submarine topographic barriers to the zonal flow and have a realistic magnitude of the Reynolds-stress divergence (see e.g. the POP model in Section 58.3). Eddy effects seem to be unimportant in the vertically integrated balance unless the ocean bottom is flat and the neglected Reynolds and frictional terms come into play. Then, simple transport formulas arise: for the familiar diffusive parameterization of lateral eddy-induced transports of momentum in terms of a diffusivity  $A_h$ , the zonal transport is then proportional to  $Y^3 \tau_0 / A_h$  for a current of width  $Y$ . Models with flat bottoms have a transport of the ACC of a couple of hundred sverdrups (more than 600 Sv in Bryan and Cox [1972]), reflecting ‘‘Hidaka’s dilemma’’ (Wolff *et al.*, 1991): with Reynolds and frictional stresses as the only means for removing the momentum being put into the ACC belt by wind stress, either unrealistically large transports are obtained or unrealistically large eddy viscosities have to be considered. In conclusion, realistic models of the ACC must include topographic effects in order to satisfy the overall

<sup>2</sup> We work with the Boussinesq approximation. Pressure and stresses are divided by a constant reference density.

balance of momentum in the presence of realistic transports.

If, in addition to the assumptions of smallness of  $R_i$  and  $\tau_i$ , the flow is adiabatic, then the meridional transport in each layer must vanish,  $\bar{V}_i = 0$ , and we find that the interfacial form stress  $\overline{\eta_i^* p_{ix}^*}$  is vertically constant and equal to  $\tau_0$  (and the bottom form stress),

$$\overline{\eta_i^* p_{ix}^*} \simeq \tau_0, \quad i = 1, 2. \quad (58.3)$$

Assuming that only transient eddies (denoted by a prime) contribute, and equating the zonal pressure gradient to the northward geostrophic velocity,  $f v'_g = p'_x$ , and the layer-thickness fluctuation to the (potential) density anomaly,  $\eta' = \rho' / \bar{\rho}_z$ , we recover the Johnson–Bryden relation (Johnson and Bryden, 1989)

$$f \frac{\overline{v' \rho'}}{\bar{\rho}_z} = \tau_0, \quad (58.4)$$

according to which the northward eddy density flux  $\overline{v' \rho'}$  (or, loosely speaking, the eddy heat flux), normalized by the mean density gradient  $\bar{\rho}_z$ , in the circumpolar belt of the ACC is of the size of the zonal wind stress  $\tau_0$ . This simple formula clearly shows the importance of eddies in the dynamics. It established one of the most celebrated models of the ACC transport. On parameterizing the transient density flux by a gradient form,  $\overline{v' \rho'} = -\kappa \rho_y$ , and using the thermal wind,  $f U_z = g \rho_y$ , the relation does indeed become prognostic for the zonal shear of the current with current profile  $U = \bar{u}(z)$ , thus relating the transport  $T = \int_{z_r}^0 U(z) dz$  (relative to some reference level  $z_r$ ) to the zonally averaged wind stress  $\tau_0$  and the eddy diffusivity  $\kappa$ , as will be discussed further in Section 58.2.1

The action of eddies not only is manifested in the interfacial form stress, but also implies a lateral eddy transport of momentum (the Reynolds-stress term), and these combine to give the transport of potential vorticity (PV)  $q$ . A more precise formulation of the momentum balance than (58.4) is thus expressed as a balance between the eddy PV flux and the vertical divergence of the frictional stress  $\tau$  in the water column (Marshall *et al.*, 1993). In a flat-bottom ocean or the ocean part above the highest topographic barrier along the zonal path of averaging, with adiabatic conditions as manifested in quasi-geostrophic (QG) models, the balance is written as

$$-\frac{\partial}{\partial y} \overline{u' v'} + f \frac{\partial}{\partial z} \frac{\overline{v' \rho'}}{\rho_z} = \overline{v' q'} = -\frac{\partial \tau}{\partial z}. \quad (58.5)$$

Equation (58.4) is in fact the consequence of (58.5) if the Reynolds-stress divergence is small and significant frictional effects are absent below the Ekman layer. Notice that, outside the Ekman layers at the top and bottom of the ocean, the frictional stress should vanish, thus implying that  $\overline{v' q'} = 0$ . The momentum balance in the form (58.5) is the

center point of the discussion of QG dynamics and eddy parameterizations in Section 58.2.2. Incidentally, the eddy PV flux can be expressed as the divergence of a flux in the plane spanned by the meridional and vertical directions,  $\overline{v'q'} = \nabla \cdot \mathbf{F}$ , with the Eliassen–Palm flux vector

$$\mathbf{F} = (-\overline{u'v'}, \overline{f v' \rho'} / \bar{\rho}_z) \quad (58.6)$$

used in Section 58.3. This property is a severe hinderance of parameterizing the PV flux: the parameterized form must accomplish the integral properties of the divergence in order to be able to accomplish the balance of momentum. Parameterizations of the momentum flux  $\overline{u'v'}$  or the density flux  $\overline{v' \rho'}$  do not suffer from such constraints. It should be mentioned, however, that no meaningful parameterizations of  $\overline{u'v'}$  (with up-gradient transport) are known.

The above concepts neglect many processes that might be important in numerical simulations of zonal currents or the ACC itself. A more complete theory is developed in Section 58.3, where the incorporation of thermohaline effects (diapycnal mixing) and the influence of topography are considered. Both effects can be identified in the simple model above. Topographic effects are seen in the presence of the standing contribution to the interfacial stress and in the bottom form-stress term. Furthermore, if there is exchange of mass between the layers, implying conversion of water masses,  $\bar{V}_i$  equals the net rate of exchange with the neighboring layers (the integral of the divergence of diapycnal transport south of the respective latitude), which implies diabatic interior effects and surface fluxes of density and, at the same time, a non-zero vertical divergence of the interfacial form stress. The thermohaline forcing of the zonal flow is thus hidden in the Coriolis force, or, equivalently, in the meridional overturning streamfunction.

## 58.2 Mixing–transport relations in flat-bottom oceans

The formulation of a complete theory capable of predicting the absolute transport of the ACC is a formidable challenge. Such a theory would need to account for wind and buoyancy forcing, stratification, the effects of eddy fluxes in the momentum and buoyancy budgets, and interactions between the strong deep currents and bottom topography. Some insight can be gained into the factors controlling the transport of the ACC by appealing to a variety of simpler models.

### 58.2.1 Simple Johnson–Bryden models

Disregarding the standing-eddy contribution as in (58.4) – and other terms that result when topography is present and the mean flow is not completely zonal – the transport theory combines the balance of zonal momentum

with parameterizations of the density flux, as indicated above. This results in

$$\kappa \frac{f^2}{N^2} U_z = \tau_0. \quad (58.7)$$

Apparently,  $A_u = \kappa f^2 / N^2$  defines a diffusivity for vertical momentum transfer achieved by lateral density diffusion. Such an equivalence was previously pointed out by Rhines and Young (1982), Olbers *et al.* (1985), and others. Johnson and Bryden (1989) used Green’s form (Green, 1970) of the diffusivity  $\kappa = \alpha \ell^2 |f| / \sqrt{\mathcal{R}_i}$ . It is obtained for a baroclinically unstable flow, where  $\mathcal{R}_i = N^2 / U_z^2$  is the local Richardson number,  $\ell$  is a measure of the eddy-transfer scale, and  $|f| / \sqrt{\mathcal{R}_i}$  is a growth rate (actually applying to Eady’s model). The constant  $\alpha$  measures the level of correlation between  $v'$  and  $\rho'$  in the density flux ( $\alpha = 0.015 \pm 0.005$  according to Visbeck *et al.* [1997]). The shear of the zonal flow and wind stress are then related by

$$\alpha \frac{|f|^3}{N^3} \ell^2 U_z^2 = \tau_0. \quad (58.8)$$

Johnson and Bryden’s results are obtained by equating the turbulence scale  $\ell$  to the baroclinic Rossby radius  $\lambda = Nh / (|f| \pi)$ . For  $\ell = \pi^2 \lambda$  we obtain their estimate of the shear:

$$U_z = \frac{N}{|f|} \left( \frac{\tau_0}{\pi^3 \alpha \lambda h} \right)^{1/2} = \left( \frac{\tau_0 / \rho_0 N(z)}{\pi^2 \alpha h^2 |f|} \right)^{1/2}. \quad (58.9)$$

The first relation was used by Johnson and Bryden (1989), with  $\lambda$  taken to be a measure of the (vertically constant) bulk Rossby radius, and shows that the shear is proportional to the local Brunt–Väisälä frequency  $N(z)$ . More importantly, the shear is proportional to the square root of the wind-stress amplitude  $\tau_0$ . In the following we use a local Rossby radius and an exponential Brunt–Väisälä frequency profile,  $N(z) = N_0 \exp[z / (2d)]$ . With  $\tau_0 = 0.2 \text{ m}^2 \text{ s}^{-2}$ ,  $h = 3500 \text{ m}$ ,  $N_0 = 1.4 \times 10^{-3} \text{ s}^{-1}$ ,  $d = 2500 \text{ m}$ , and a width  $Y = 600 \text{ km}$  of the ACC, integration of (58.9) yields a transport of 82 Sv relative to the bottom.

Visbeck *et al.* (1997) suggested that, in the presence of differential rotation, the eddy transfer may be restricted by the Rhines scale  $\sqrt{U/\beta}$  rather than the Rossby radius.<sup>3</sup> With  $\ell = \sqrt{U/\beta}$  we find a cubic relation between  $\tau_0$  and the velocity,

$$U U_z^2 = \frac{\tau_0 \beta N^3(z)}{\alpha |f|^3}. \quad (58.10)$$

For the exponential  $N(z)$  this is easily integrated. A transport of 67 Sv relative to the bottom and a total transport

<sup>3</sup> Actually, to be Galileian invariant, the  $U$  in the Rhines scale must be a measure of the square root of the kinetic energy of fluctuations of the jet, i.e. the assumption  $\sqrt{u'^2} \sim U$  is hidden within the concept.

of 124 Sv are obtained for the above set of parameters. In this model the transport would only mildly increase with increasing magnitude of the wind stress, as  $\tau_0^{1/3}$ . Notice, however, the dependence on  $\beta$  in this regime.

If eddy mixing of PV is down the mean PV gradient,  $\overline{v'q'} = -k\bar{q}_y$ , the vanishing of the eddy PV flux implies zero PV gradient, as suggested in the preceding section on the basis of the balance of momentum. This results in  $\bar{q}_y = 0$ , and thus homogeneous mean PV. Observations do indeed show that isopycnal vorticity gradients are small (compared with the planetary vorticity gradient  $\beta$ ) in and north of the Antarctic Current regime (Marshall *et al.*, 1993). Furthermore, in that investigation a linear relation between the large-scale PV and density was found to exist, namely  $f\rho_z = a + b\rho$ , with  $d = |f|/b$ , the e-folding scale of the density field. This implies an exponential  $N(z)$ , as assumed before, and it also imposes a constraint on the current shear,

$$U_{zz} - \frac{U_z}{d} = \beta \frac{N^2}{f^2}, \quad (58.11)$$

which is obtained by taking the meridional derivative of  $f\rho_z = a + b\rho$  and the thermal wind relation  $fU_z = g\rho_y$ . Vertical integration immediately leads to the velocity profile and the transport, expressed in terms of the vertical shear at some level  $z_0$ . A more meaningful interpretation is found if (58.11) is reformulated by inserting (58.7), which yields a constraint on the vertical profile of the diffusivity  $\kappa$ ,

$$\frac{\partial}{\partial z} \frac{1}{\kappa} = \frac{\partial}{\partial z} \frac{f^2}{N^2 A_v} = \frac{\beta}{\tau_0}. \quad (58.12)$$

Apparently, the assumption of a homogeneous PV state sets the vertical profile of the lateral diffusivity of density. Notice that  $\beta$  rules the vertical profile of the diffusivity and that  $\tau_0$  represents the vertically constant flux of momentum in the water column which equals the wind stress. In this model the shear consists of two parts,

$$U_z = \frac{N^2}{f^2} \left( \frac{\tau_0}{\kappa_0} + \beta(z - z_0) \right), \quad (58.13)$$

where  $\kappa_0 = \kappa(z_0)$ . The first contribution is directly wind-driven. The second contribution is driven by the eddies which homogenize the associated PV. The transport (relative to the bottom) of the latter is fairly small and westward ( $\approx -2$  Sv), whereas the first part contributes 39 Sv for our standard values and a diffusivity of  $\kappa_0 = 1000 \text{ m}^2 \text{ s}^{-1}$  at  $z_0 = -1000$  m. Following (58.12),  $\kappa$  then increases to  $1200 \text{ m}^2 \text{ s}^{-1}$  at depth 3500 m.

As is evident from (58.9), (58.10), and (58.13) the dependence of the baroclinic transport on the amplitude of the wind stress and the Brunt–Väisälä frequency is generally governed by the degree of non-linearity of the eddy-flux parameterization. It should be kept in mind that only

transient-eddy effects are taken into account in these parameterizations. It is thus not surprising that numerous attempts with numerical models, whether adiabatic or full potential energy but with consideration of topography, failed to verify the prediction of the square-root dependence,  $\mathcal{T} \sim \tau_0^{1/2}$ , resulting from a Green parameterization of the diffusivity  $\kappa$ . Attempts also with the cubic relation,  $\mathcal{T} \sim \tau_0^{1/3}$ , resulting from the Rhines-scale approach, were without success. However, there is only a very restrictive range of applicability of (58.4): it is valid only under adiabatic conditions, only for the water column below the Ekman layer and above the highest topography in the circumpolar belt, and only if Reynolds stresses are small in the balance of zonal momentum. It should also be pointed out that, in the above consideration, the stratification is prescribed by the Brunt–Väisälä frequency  $N(z)$ . However, since this is established by thermohaline forcing, diffusion, and the transports of heat and salt, it should depend indirectly on the wind stress as well. This question is posed in Section 58.3.3.

### 58.2.2 The quasi-geostrophic view

The relation (58.5) is the QG form of the time-and-zonal-mean-momentum balance for zonal flow over a flat terrain. The QG dynamics are governed by the balance equation

$$\frac{\partial q_i}{\partial t} + \mathcal{J}(\psi_i, q_i) = \frac{\partial q_i}{\partial t} + \nabla \cdot \mathbf{u}_i q_i = F_i \quad (58.14)$$

for the QG potential vorticity (QPV)  $q_i$ , driven by vorticity sources  $F_i$ . The balance is written for a stack of layers as in the conceptual model in Section 58.1 (however, with immiscible layers one has  $V_i \equiv 0$ ), thus  $\psi_i$  is the streamfunction of the geostrophic current in the  $i$ th layer ( $i = 1, \dots, n$ ),  $u_i = -\psi_{iy}$ , and  $v_i = \psi_{ix}$  are the velocities, and the QPV is given by

$$q_i = \nabla^2 \psi_i + \frac{f_0}{H_i} (\eta_i - \eta_{i-1}) + f \quad (58.15)$$

with  $f = f_0 + \beta y$  for flow on a  $\beta$ -plane. As before, the  $\eta_i$  are the interface depths (in fact, only deviations from a mean layer thickness  $H_i$  matter). They may be expressed in terms of the streamfunctions; in most applications a rigid-lid condition is used at the top, thus  $\eta_0 \equiv 0$ . We discuss properties of a two-layer model in which the elevation of the interface is  $\eta = \eta_1 + H_1 = (f_0/g')(\psi_2 - \psi_1)$ . We will examine consequences of parameterizations of the eddy transport  $\overline{v'q'_i}$  of QPV and  $\overline{v'\eta'}$  of mass for the zonal transport in a channel flow that is driven by a zonal wind stress in the top layer, and has bottom friction but no interfacial friction.

The numerical model applies to a flow in a two-layer channel of length  $X = 4000$  km and width  $Y = 1500$  km on a  $\beta$ -plane the layers have depths  $H_1 = 1000$  m and  $H_2 = 4000$  m. The balance of QPV includes friction terms

Table 58.1. Some integral quantities of the numerical experiment:  $H_i \mathcal{T}_i$  is the transport in the  $i$ th layer, and  $E_i^{\text{kin}}$  and  $E^{\text{pot}}$  are the mean kinetic and potential energies of the flow

Experiment	$H_1 \mathcal{T}_1$ ( $10^6 \text{ m}^3 \text{ s}^{-1}$ )	$H_2 \mathcal{T}_2$ ( $10^6 \text{ m}^3 \text{ s}^{-1}$ )	$E_1^{\text{kin}}$ ( $\text{m}^3 \text{ s}^{-2}$ )	$E_2^{\text{kin}}$ ( $\text{m}^3 \text{ s}^{-2}$ )	$E^{\text{pot}}$ ( $\text{m}^3 \text{ s}^{-2}$ )
EFB	377	949	62	93	700
EBO	275	950	28	69	65
WFB	−299	−946	29	75	154

$F_i = \mathbf{k} \cdot \nabla \times \tau_i / H_i - A_{\text{hyp}} \nabla^6 \psi_i$  where  $\tau_1$  is the wind-stress vector, and  $\tau_2$  is the frictional bottom stress. Anticipating results from a numerical model, subgrid-scale effects are modeled by biharmonic lateral friction with hyperviscosity  $A_{\text{hyp}} = 10^{10} \text{ m}^4 \text{ s}^{-1}$ . It reflects the parameterization of subgrid momentum transport and serves as energy and enstrophy dissipation. The channel has a central latitude of  $60^\circ \text{S}$ , with  $f_0 = -1.263 \times 10^{-4} \text{ s}^{-1}$  and reduced gravity  $g' = 0.02$  so that the internal Rossby radius  $\lambda = \{g' H_1 H_2 / [f_0^2 (H_1 + H_2)]\}^{1/2}$  is 32 km. Lateral boundary conditions  $\nabla^2 \psi_i = 0$  and  $\nabla^4 \psi_i = 0$  on both walls (the latter establishes zero momentum flux) and integral auxiliary conditions (McWilliams, 1977) are standard. A fourth-order-accurate formulation of the Jacobian (Arakawa, 1966) turned out to be necessary in order to compute the second-order eddy balances correctly (Wolff *et al.*, 1993). The resolution of the model grid is 10 km. The wind stress is zonal and zonally constant,

$$\tau_1 = \tau_0 \sin\left(\frac{\pi(y + Y/2)}{Y}\right) \quad (58.16)$$

with amplitude  $\tau_0 = \pm 10^{-4} \text{ m}^2 \text{ s}^{-2}$  for eastward or westward forcing. In the experiments discussed here the frictional stress at the bottom is taken as a linear functional of the bottom velocity, i.e.  $\tau_2 = -\epsilon H_2 \mathbf{u}_2$ , where  $\epsilon$  is the corresponding coefficient of linear bottom friction (we take  $\epsilon = 10^{-7} \text{ s}^{-1}$ ).

Numerical solutions obtained with this model have been described by Wolff and Olbers (1989), Wolff *et al.* (1991), Olbers *et al.* (1997, 2000), and Ivchenko *et al.* (1997). Other important similar experiments are reported in McWilliams *et al.* (1978). These applications embrace a large suite of flat-bottom experiments (also with other forcings and non-linear bottom friction) and experiments with topography in the deep layer (not considered in the QG dynamics described above). Here, we concentrate the discussion on flat-bottom cases: a typical  $\beta$ -plane case (EFB), an  $f$ -plane case (EBO), both forced by eastward wind, and a westward-forced  $\beta$ -plane case (WFB). All experiments were initially integrated for 7 years starting from the state of rest. At this time the currents in EFB and EBO are identical and WFB mirrors exactly the eastward cases: a wide lami-

nar flow matching the meridional scale of the wind stress. The zonal velocity profile follows the smooth profile of the applied wind stress in all cases with maximum velocities of about  $40 \text{ cm s}^{-1}$  and the kinetic and potential energies are identical. The flow field was then perturbed and, because the states were unstable with respect to this disturbance, the flow changed dramatically to a fully turbulent field when the disturbance was advected with the main current and also propagated. The integration was continued for a total of 110 model years and, judging by the form of the evolution with time of the kinetic and potential energies, the flow can be considered to be in a statistically steady state about 4 years after the introduction of the disturbance. Transports in the layers and energies in the quasi-steady state can be found in Table 58.1.

Figures 58.1–58.3 show instantaneous total streamfunction fields and the corresponding eddy streamfunctions (defined as deviations from the time mean) at the end of the experiment. The narrow jet in EFB with a characteristic meridional scale of 400–500 km (which is much larger than the Rossby radius and much smaller than the wind-stress scale) is seen to meander significantly, with stronger meanders appearing in the upper layer. Along the entire length of the basin there are typically five large-scale wave-like disturbances of the main jet; the wavelength is thus approximately 800 km. The maximum velocity of the mean eastward jet is about  $60 \text{ cm s}^{-1}$ . The  $f$ -plane experiment EBO has a much more sluggish flow. Zonal waves are present but cannot be attributed to a dominant scale. Also, the currents in the  $\beta$ -plane experiments EFB and WFB differ quite significantly. The westward-flow WFB has a current that is not a narrow jet, but wide and smooth with a typical meridional scale equal to the basin width, and significantly smaller velocities on the current axis.

The EFB eddies form a regular chain in the vicinity the center of the jet (particularly in the lower layer). The eddies have an ellipsoidal form, leaning into the direction of the jet. This pattern causes the Reynolds-stress convergence and thus the concentration of the jet (Holland and Haidvogel, 1980). The eddy field in EBO is rather weak compared with the  $\beta$ -plane cases; the eddies have no dominant scale. In both cases, the eddies have a strong barotropic vertical

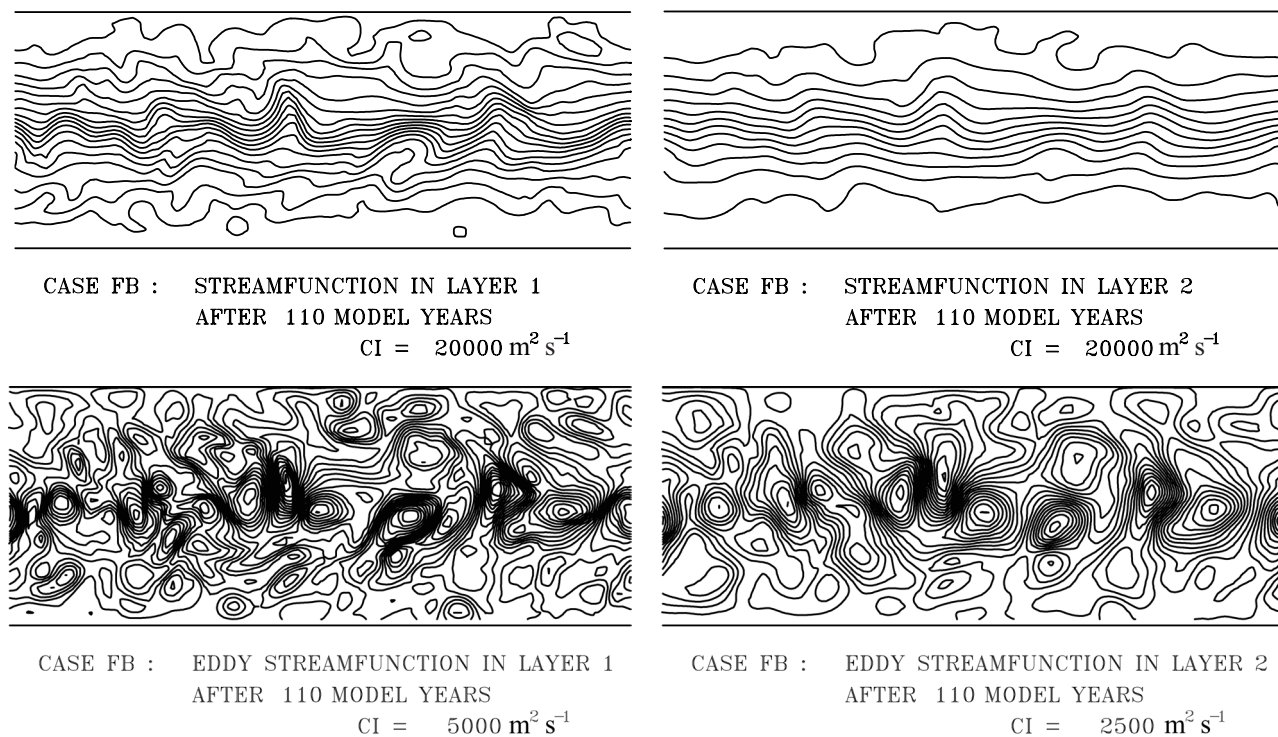


Fig. 58.1. Instantaneous (upper panels) and eddy streamfunctions (lower panels) for the experiment EFB (flat bottom,  $\beta$ -plane, eastward wind), the upper layer is on the left and the lower layer is on the right. Contour intervals are  $2 \times 10^4 \text{ m}^2 \text{ s}^{-1}$  for the upper panels and  $5 \times 10^3 \text{ m}^2 \text{ s}^{-1}$  for the lower-left-hand panel and  $2.5 \times 10^3 \text{ m}^2 \text{ s}^{-1}$  for the lower-right-hand panel.

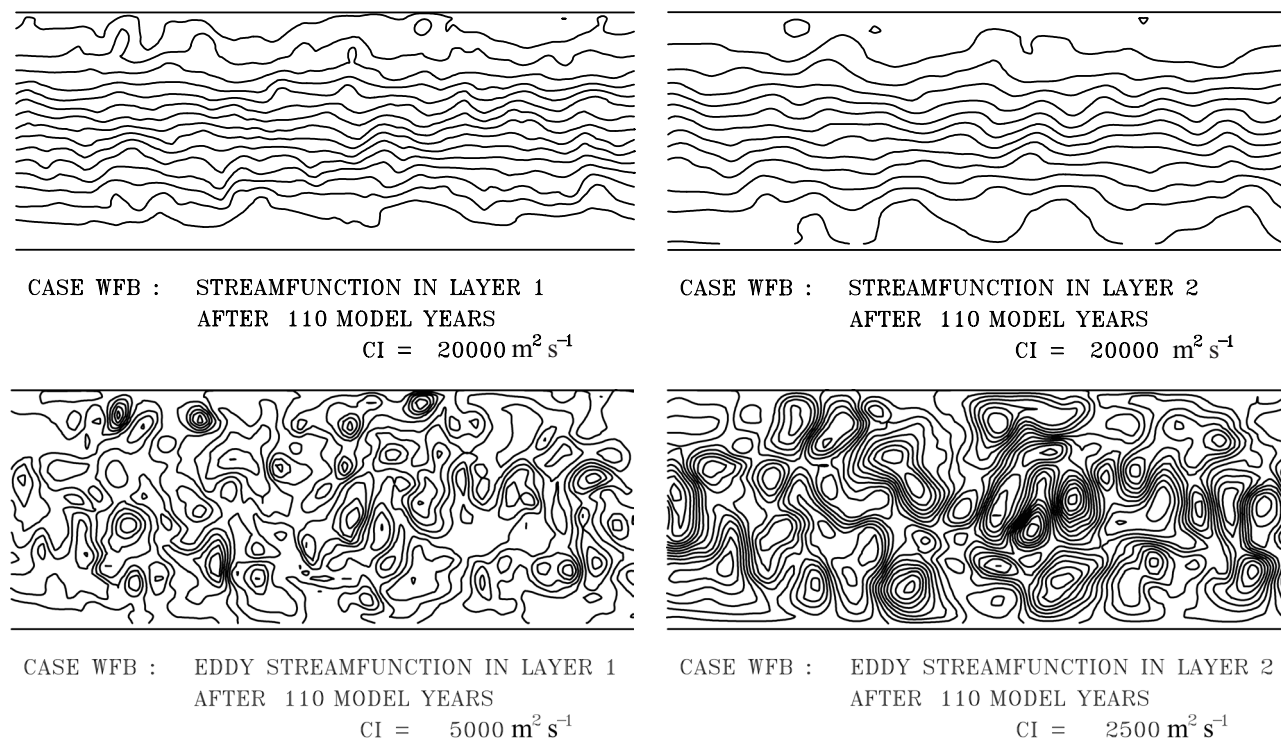


Fig. 58.2. As Fig. 58.1, for the experiment EB0 (flat bottom,  $f$ -plane, eastward wind).

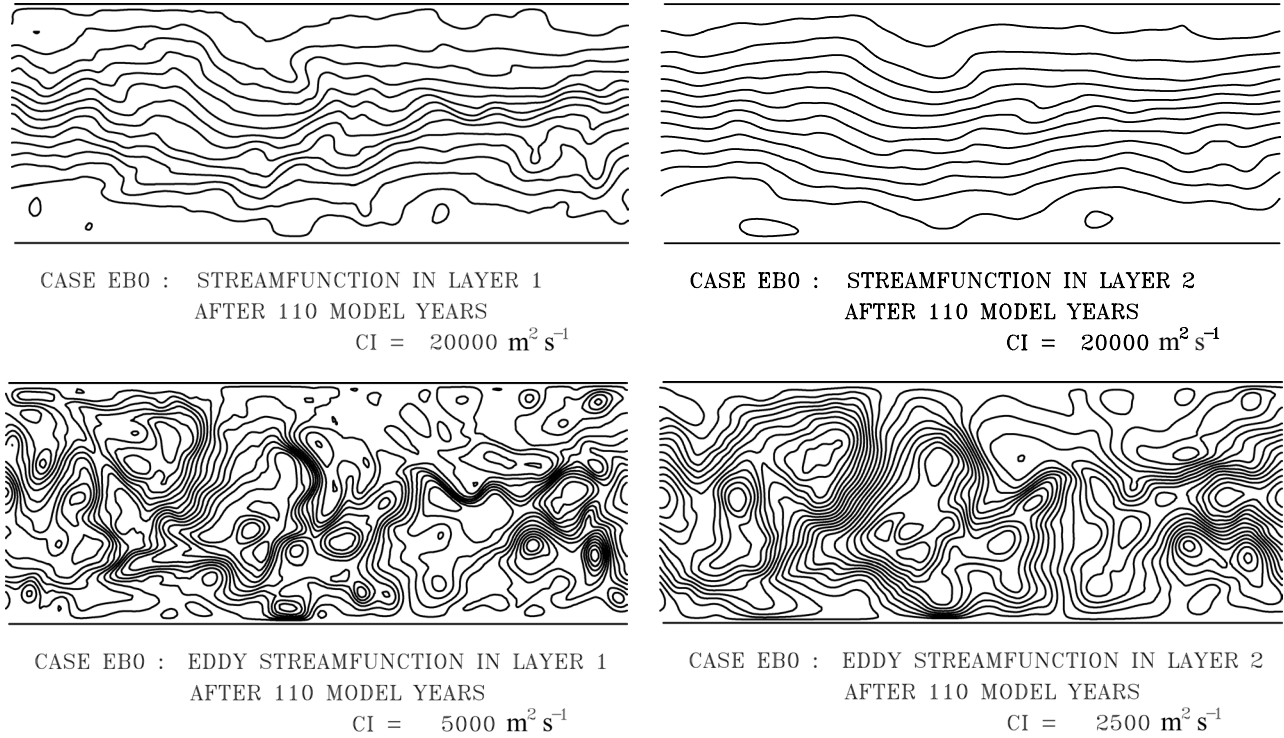


Fig. 58.3. As Fig. 58.1, for the experiment WFB (flat bottom,  $\beta$ -plane, westward wind).

structure. In WFB the eddy field appears chaotic and eddies are scattered all over the channel. In contrast to EFB, the mesoscale eddies in WFB are much stronger in the lower layer than in the upper layer.

Figure 58.4 shows the profiles of the time-and-zonally averaged zonal velocity. Although the total transports of the three cases are similar (see Table 58.1), we find a significant difference in the structure of the flow. The concentrated jet in EFB with a width of about 400 km is flanked by side lobes having a similar width. The  $f$ -plane flow is wide and smooth with a typical meridional scale equal to the basin width – it mirrors almost exactly the sinusoidal profile of the wind stress. The westward flow has a very similar structure. The velocities in the center of the jet are significantly smaller than those in the strong jet in EFB. The flow is unstable in both eastward cases, whereas for EFB the mean shear is above the critical value of Phillip’s inviscid linear instability criterion ( $S = \bar{u}_1 - \bar{u}_2 > \beta \sqrt{g'H_2/f_0^2}$  or  $S < -\beta \sqrt{g'H_1/f_0^2}$  for eastward and westward flow, respectively; the criterion is not exactly applicable since the current profiles are not meridionally uniform, see e.g. Pedlosky [1987]).

Further time-and-zonal mean fields are presented in the above-cited articles in which the balances of the most important properties (momentum, enstrophy,

energies) were investigated as well. The momentum balance

$$-H_i \overline{v'_i q'_i} = \bar{\tau}_i \quad (58.17)$$

is of relevance for the following discussion (the overbar indicates the time-and-zonal average, as before). It is the layer integral of (58.5), or derived from (58.14) using  $F_i = -(1/H_i) \partial \tau_i / \partial y$  (omitting the hyperviscous terms),  $\bar{\tau}_i(y)$  is the prescribed wind stress, and  $\bar{\tau}_2 = -\epsilon H_2 \bar{u}_2$  is the frictional bottom stress. It is immediately evident from the form of the QPV flux (see Fig. 58.5) that the total QPV flux, integrated over the depth and width of the channel, vanishes,

$$\int_{-Y/2}^{Y/2} (H_1 \overline{v'_1 q'_1} + H_2 \overline{v'_2 q'_2}) dy = 0. \quad (58.18)$$

This property guarantees the conservation of momentum: the momentum input by wind in the top layer is extracted totally by friction at the bottom,

$$\int_{-Y/2}^{Y/2} (\bar{\tau}_1 - \epsilon H_2 \bar{u}_2) dy = 0. \quad (58.19)$$

The constraint (58.18) is a non-local property, which puts a heavy burden on any parameterization of the eddy QPV flux since violation would spoil (58.19). Evidently, the relation (58.19) fixes the transport in the bottom layer entirely in

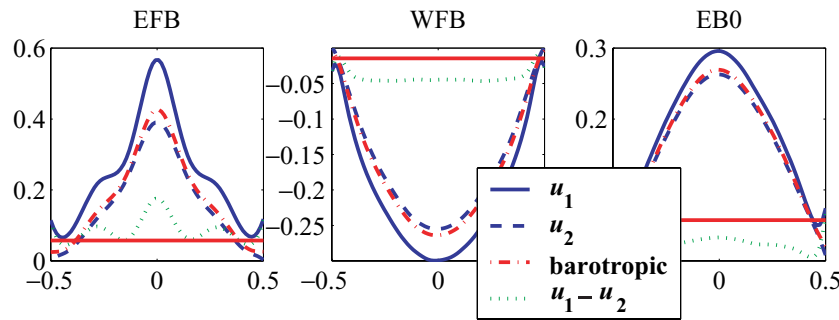


Fig. 58.4. Time and zonal mean profiles of the velocity  $\bar{u}_1$  (full),  $\bar{u}_2$  (dashed), the barotropic velocity  $C = (H_1\bar{u}_1 + H_2\bar{u}_2)/H$  (dash-dotted) and the vertical shear velocity  $S = \bar{u}_1 - \bar{u}_2$  (dotted) for EFB, WFB, and EBO as functions of the scaled meridional latitude  $y/Y$ . The critical phase speeds  $\beta\sqrt{g'H_2/f_0^2}$  for eastward flow and  $-\beta\sqrt{g'H_1/f_0^2}$  for westward flow are included as straight lines for EFB and WFB. Units are  $\text{m s}^{-1}$ .

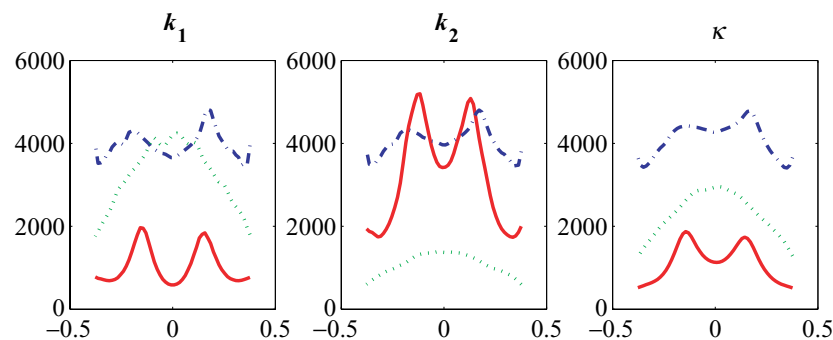


Fig. 58.5. Eddy diffusivities  $k_i$  of the potential vorticity flux and  $\kappa$  of layer thickness, as functions of the scaled meridional latitude  $y/Y$ , in units of  $\text{m}^2 \text{s}^{-1}$ . Boundary layers are omitted. EFB (full), WFB (dotted), and EBO (dash-dotted).

terms of the applied wind stress (see the next section). Thus, all three experiments should have the same value of the bottom-layer transport (see Table 58.1; differences are due to finite-time averaging).

The layer gradients of mean QPV  $\bar{q}_i$  reveal the well-known property of the differing signs in the upper and lower layers in all cases; thus the general condition of baroclinic instability is satisfied. It is important for the purposes of the present study that the QPV flux is down-gradient in all cases, so the numerically determined diffusivities

$$k_i = -\overline{v'_i q'_i} / \frac{\partial \bar{q}_i}{\partial y} \quad (58.20)$$

are positive throughout. The profile of  $k_i$  is rather complex. A local minimum is observed in the center of the jet for the eastward cases EFB and EBO and maximum values are found on the flanks of the jet. In contrast, the diffusivities of the WFB case possess a single maximum in the center; the structure is sinusoidal, as are the current profiles.

Another prominent example of a down-gradient flux is the eddy-induced mass flux (or layer-thickness flux)  $\overline{v'_i \eta'}$  such that

$$\kappa = -\overline{v'_i \eta'} / \frac{\partial \bar{\eta}}{\partial y} \quad (58.21)$$

is positive as well. The eddy flux  $\overline{v'_i \eta'}$  (which equals  $\overline{v'_2 \eta'}$ ) is called the “bolus” transport velocity in isopycnal formulations of mean transport equations for tracers (see e.g. Gent and McWilliams [1990], and Gent *et al.* [1995]). In the momentum balance (58.17) the lateral eddy mass transport is equivalent to a vertical momentum transport and a parameterization of the form (58.21) then implies vertical transport of horizontal momentum with a diffusion coefficient  $\kappa H_i f_0^2 / g'$  (see also Eq. (58.7)). In the layer framework this appears as interfacial friction. In truly large-scale flow where the respective contributions of relative vorticity can be neglected in the QPV flux as well as in the mean QPV gradient, the main difference between QPV diffusion and thickness diffusion is found in the presence of the eddy transport of planetary vorticity,  $k_i \beta$ , in (58.20).

Note that the coefficients for QPV diffusion in the layers are different and have a clear ordering,  $k_2 > k_1$  for eastward flow and  $k_2 < k_1$  for westward flow on the  $\beta$ -plane. In the  $f$ -plane case the coefficients have similar magnitudes (within numerical errors from finite-time averaging, they are equal). The diffusivity  $\kappa$  for layer thickness has a similar structure to the  $k_i$ , with less prominent central valleys. It is shown in Olbers *et al.* (2000) that known parameterization concepts based upon baroclinic instability (Green, 1970; Stone, 1972) or homogeneous  $\beta$ -plane turbulence (Larichev and Held, 1995; Held and Larichev, 1996) do not explain the double-peak structure of the eastward cases. We would like to point out that the following analysis does not consider (58.20) or (58.21) a physically motivated parameterization. For this task the diffusivities must be related to mean-field quantities and regime-robust universal coefficients. We simply investigate the implication of the positivity of the  $k_i$  and  $\kappa$  for the channel transport.

### The zonal transport based on effective diffusivities

There is a straightforward way to utilize the parameterized momentum balance (58.5), written now in the form

$$k_i \frac{\partial \bar{q}_i}{\partial y} = \frac{\bar{\tau}_i}{H_i} \quad (58.22)$$

with the help of (58.20), to obtain explicit relations between the transports in QG models and the external parameters, i.e. the wind stress, the diffusion and friction coefficients, and the channel dimensions. On inserting the expression (58.15) of the QPV into (58.22), we find

$$\begin{aligned} -\frac{\partial^2 \bar{u}_1}{\partial y^2} - \frac{f_0^2}{g' H_1} (\bar{u}_2 - \bar{u}_1) + \beta &= \frac{\tau_1}{k_1 H_1}, \\ -\frac{\partial^2 \bar{u}_2}{\partial y^2} + \frac{f_0^2}{g'' H_2} (\bar{u}_2 - \bar{u}_1) + \beta &= -\frac{\epsilon}{k_2} \bar{u}_2. \end{aligned} \quad (58.23)$$

On integrating (58.23) across the channel and utilizing free-slip conditions for simplicity at the walls, we obtain a set of equations for the layer transports (per unit depth)

$$\mathcal{T}_i = \int_{-Y/2}^{Y/2} dy \bar{u}_i. \quad (58.24)$$

These take the form

$$\begin{aligned} -\frac{f_0^2}{g'} (\mathcal{T}_2 - \mathcal{T}_1) &= \frac{\mathcal{W}}{K_1} - \beta H_1 Y, \\ \frac{f_0^2}{g''} (\mathcal{T}_2 - \mathcal{T}_1) + \frac{\epsilon H_2}{K_2} \mathcal{T}_2 &= -\beta H_2 Y, \end{aligned} \quad (58.25)$$

with integrated wind stress  $\mathcal{W}$  and effective (weighted) diffusivities  $K_i$ , defined by

$$\begin{aligned} \mathcal{W} &= \int_{-Y/2}^{Y/2} \tau_1 dy, & \frac{\mathcal{W}}{K_1} &= \int_{-Y/2}^{Y/2} \frac{\tau_1}{k_1} dy, \\ \frac{\mathcal{T}_2}{K_2} &= \int_{-Y/2}^{Y/2} \frac{\bar{u}_2}{k_2} dy. \end{aligned} \quad (58.26)$$

The presence of the eddy fluxes requires the conditions of baroclinic instability to be fulfilled. In terms of the transport variables  $\mathcal{T}_i$ , these are written as

$$\mathcal{T}_1 - \mathcal{T}_2 \begin{cases} > g' \beta Y H_2 / f_0^2 & \text{for eastward flow,} \\ < -g' \beta Y H_1 / f_0^2 & \text{for westward flow,} \end{cases} \quad (58.27)$$

which implies that  $\mathcal{W}/(\beta Y H) > K_1$  for  $\mathcal{W} > 0$  and  $|\mathcal{W}|/(\beta Y H) < K_2$  for  $\mathcal{W} < 0$ , as a consequence of the transport relations (58.25). These bounds of the effective diffusivities are satisfied in our experiments.

Surprisingly, the linear set of equations (58.25) yields solutions for the transports  $\mathcal{T}_i$  that seem to be non-zero (arising from the  $\beta$  terms) for vanishing forcing  $\tau_1$ . One must, however, remember that the diffusivities  $K_1$  and  $K_2$  are not independent but must obey the constraint (58.18), which, by use of (58.19), is equivalent to the condition of the total momentum balance of the channel, which determines the deep transport,  $\mathcal{T}_2 = \mathcal{W}/(\epsilon H_2)$ . On summing (58.25) and using (58.26) and (58.19), this condition assumes the particular form

$$\beta Y H = \left( \frac{1}{K_1} - \frac{1}{K_2} \right) \mathcal{W}, \quad (58.28)$$

where  $H = H_1 + H_2$  is the total depth of water. This shows that a proper choice of the diffusivities in fact converts the  $\beta$  terms in (58.25) into terms proportional to the forcing  $\mathcal{W}$ . Notice that (58.28) implies that  $K_1 < K_2$  for eastward wind stress and  $K_1 > K_2$  for westward wind stress on the  $\beta$ -plane, as pointed out before for the numerically determined  $k_i$ . In contrast, the  $f$ -plane case has  $K_1 = K_2$ , which is also confirmed by the numerical result. Using (58.28), one easily finds the solution for the transport in the top layer:

$$\mathcal{T}_1 = \mathcal{T}_2 + \frac{g'}{H f_0^2} \left( \frac{H_2}{K_1} + \frac{H_1}{K_2} \right) \mathcal{W}, \quad (58.29)$$

where the diffusivities are still subject to the constraint (58.28). The solution is shown in Fig. 58.6 for the parameters of the three numerical experiments. The figures include as contours also the values of  $H_1 \mathcal{T}_1$  for the specific cases and the curves of the constraint (58.28). On extracting the solution  $K_1$  and  $K_2$  from the intersection, we see a good agreement with the eddy diffusivities from Fig. 58.5 in each case.

The depth profile of the QPV diffusivities is thus a consequence of the balance of momentum. With this

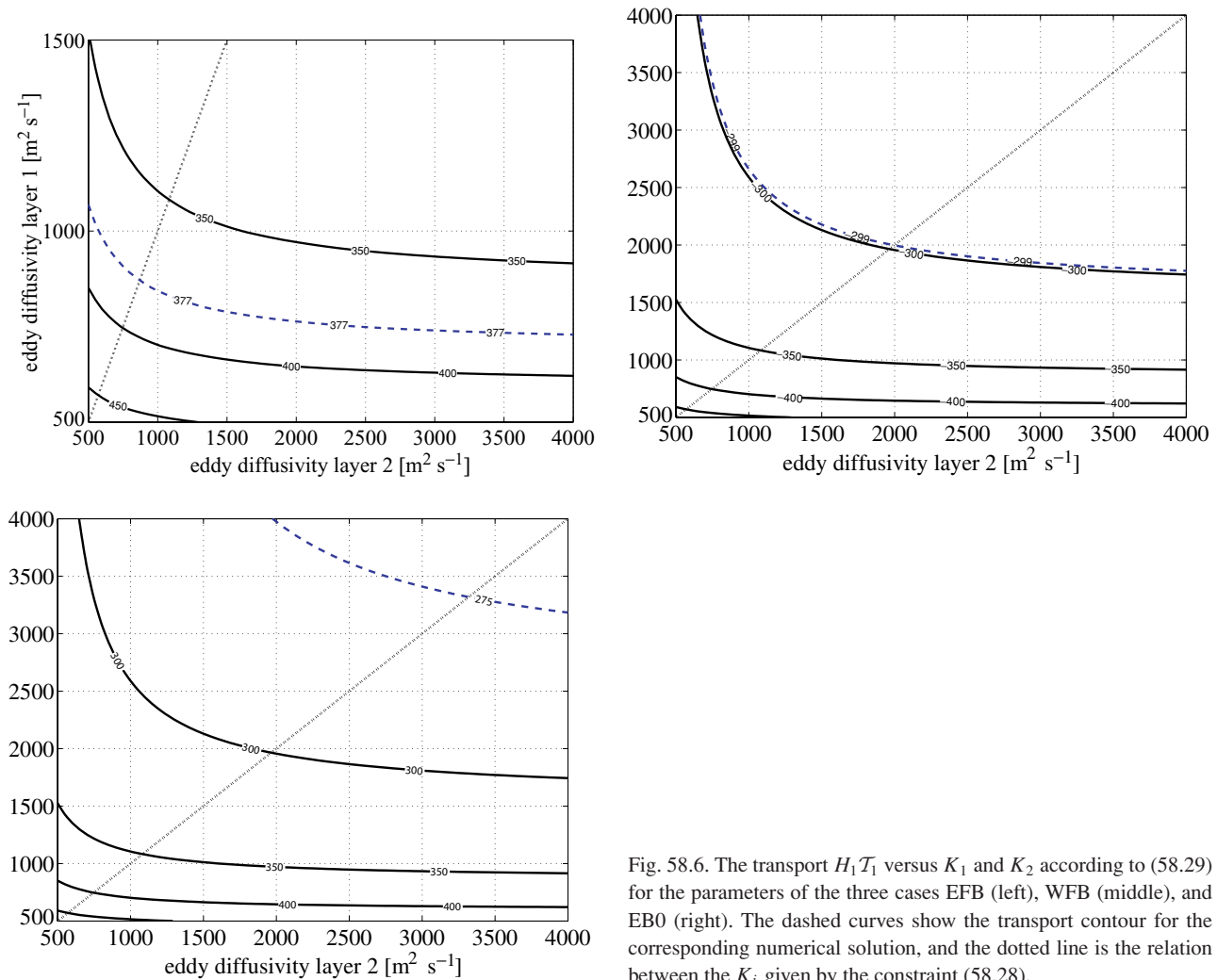


Fig. 58.6. The transport  $H_1 T_1$  versus  $K_1$  and  $K_2$  according to (58.29) for the parameters of the three cases EFB (left), WFB (middle), and EB0 (right). The dashed curves show the transport contour for the corresponding numerical solution, and the dotted line is the relation between the  $K_i$  given by the constraint (58.28).

constraint the planetary conditions enter the theory via dependence on  $\beta$ . Returning to a vertically continuous representation, the relation (58.28) implies

$$(1/K)_z \sim \beta/\tau_0, \quad (58.30)$$

which is identical to the implication (58.12) of PV homogenization, which was discussed in Section 58.2.1. Notice, however, that the two diffusivities describe different properties.

This theory can easily be extended to more than two layers. Notice that the diffusion coefficients of intermediate layers that are not in contact with the surface or the bottom do not enter explicitly since these layers are frictionless. Eddies must, however, be present to homogenize the QPV; in fact, the momentum balance (58.22) of the intermediate layers states that the QPV is constant there (see Marshall *et al.* [1993] for further demonstration with a three-layer QG model of the ACC with realistic coastlines and topog-

raphy). The intermediate layers do, however, contribute to the transport.

Utilization of the down-gradient property of the thickness flux, as indicated in (58.21), for determination of transport is possible only if the Reynolds-stress contribution to the eddy QPV flux in (58.5) or (58.17) is negligible (as assumed in Section 58.2.1). In this case, the transport equations corresponding to (58.25) are much simpler – the coefficients  $K_i$  are replaced by one value  $K$  arising from  $\kappa$ , and the  $\beta$  terms are absent. Thus, there is no constraint like (58.28), and  $T_1 - T_2 = g'W/(Kf_0^2)$ , which can be viewed as the QG form of the Johnson–Bryden relation. This approach might be applicable to WFB and EB0, but not for the eastward  $\beta$ -plane case EFB (and a large suite of other eastward cases presented in Olbers *et al.* [2000]). In this most prominent regime, being closest to the ACC conditions, we find convergence of zonal momentum by Reynolds stresses an important ingredient of the flow

characteristics, as manifested in the central jet of the EFB experiment, shown in Figs. 58.1 and 58.4.

The seemingly linear dependence of layer and total transports on the applied wind stress  $\mathcal{W}$  must be taken with care: the numerically determined diffusivities  $k_i$  and  $\kappa$  are not parameterizations; they vary if the forcing or the system parameters (channel dimensions, coefficients of friction and stratification, etc.) are changed.

**Functional relations** The structure of the flow has been analyzed by considering the functional relationship  $\bar{q}_i = G_i(\bar{\psi}_i)$  between the mean QPV  $\bar{q}_i$  and the streamfunction  $\bar{\psi}_i$  in each layer.<sup>4</sup> Such a relation trivially exists here because both fields depend only on  $y$ . In general a functional relation between  $\bar{q}_i$  and  $\bar{\psi}_i$  demands smallness of the frictional terms compared with the mean advective terms in the QPV balance (see below). Knowing  $G_i(\bar{\psi}_i)$  in fact completely determines the flow: the streamfunctions can of course be recovered by solving the differential equations

$$\nabla^2 \bar{\psi}_i + (-1)^i \frac{f_0^2}{g'H_i} (\bar{\psi}_1 - \bar{\psi}_2) + f = G_i(\bar{\psi}_i), \quad i = 1, 2. \quad (58.31)$$

Appropriate boundary conditions are  $\bar{\psi}_i = \text{constant}$  and  $\nabla^2 \bar{\psi}_i = 0$  (in agreement with the numerical model). All other boundary conditions and constraints are incorporated into the functionals  $G_i$ , in particular the values of the transports, as shown below. For a large-scale flow the relative-vorticity part can be neglected. Then (58.31) becomes an algebraic problem.

The numerical experiments indicate that the functional relationship  $G_i(\bar{\psi}_i)$  is almost linear (see Fig. 58.7 and also McWilliams *et al.* [1978]), i.e. we may write

$$\bar{q}_i = G_i(\bar{\psi}_i) = A_i \bar{\psi}_i + B_i + g_i(\bar{\psi}_i), \quad (58.32)$$

where  $A_i$  and  $B_i$  are dimensional constants and  $g_i$  a small remainder, which, moreover, may be assumed to vanish for the boundary values of the corresponding streamfunctions. It is obvious from (58.31) that the coefficients  $A_i$  and  $B_i$  are directly related to the four values of the streamfunctions at the boundaries. Specifically, the  $A_i$  are given by the transports in the two layers (or vice versa), as follows from

$$\begin{aligned} -\frac{f_0^2}{g'}(\mathcal{T}_2 - \mathcal{T}_1) + \beta H_1 Y &= -A_1 H_1 \mathcal{T}_1, \\ \frac{f_0^2}{g'}(\mathcal{T}_2 - \mathcal{T}_1) + \beta H_2 Y &= -A_2 H_2 \mathcal{T}_2. \end{aligned} \quad (58.33)$$

<sup>4</sup> In this section, the overbar indicates only the time average, i.e. there is no zonal averaging implied.

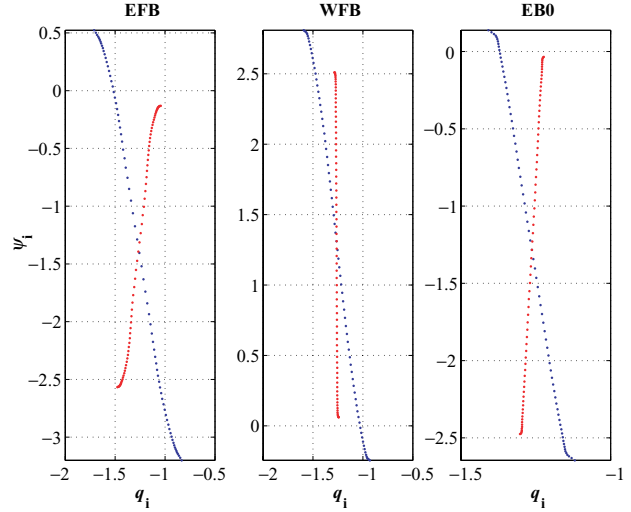


Fig. 58.7. The functional relation between streamfunction and QPV for the three experiments. The line with smaller  $\bar{\psi}$  range refers to the lower layer, units are  $10^5 \text{ m}^2 \text{ s}^{-1}$  for  $\bar{\psi}_i$  and  $10^{-4} \text{ s}^{-1}$  for  $\bar{q}_i$ .

The presence of the eddy fluxes requires that the conditions of baroclinic instability be fulfilled. In terms of the transport variables  $\mathcal{T}_i$  these are given by (58.27). It is an easy matter to prove  $A_1 < 0$  and  $A_2 > 0$  from (58.33) and (58.27). In fact, the general condition of baroclinic instability in a two-layer system may be expressed as  $\partial G_2 / \partial \bar{\psi}_2 > 0$  for eastward flow and  $\partial G_1 / \partial \bar{\psi}_1 < 0$  for westward flow, in agreement with the numerical experiments. The  $A_i$  and the diffusivities  $K_i$  are of course related:  $A_1 K_1 = -[H_1 / (\epsilon H_2)] + [g'H_1 / (Hf_0^2)](H_2 / K_1 + H_1 / K_2)^{-1}$  and  $A_2 K_2 = \epsilon$ . We would like to emphasize that all information about the flow beyond the transports is contained in the deviations  $g_i(\bar{\psi}_i)$  from the gross linear part  $A_i \bar{\psi}_i + B_i$ . Neglecting the  $g_i$  in (58.31) results in a trivial parabolic shear flow, which is a bad approximation to our numerical results of EFB.

The functionals  $G_i(\bar{\psi}_i)$  result in a complex indirect way from the forcing at the surface and friction at the bottom as well as from the eddy fluxes of QPV. A simple view may be gained by elaborating on the time-mean QPV balance,

$$\begin{aligned} \mathcal{J}(\bar{\psi}_i, \bar{q}_i) &= -\mathcal{J}(\bar{\psi}'_i, \bar{q}'_i) + \bar{F}_i = -\nabla \cdot \bar{\mathbf{u}}'_i \bar{q}'_i \\ &\quad + \mathbf{k} \cdot \nabla \times \bar{\boldsymbol{\tau}}_i / H_i. \end{aligned} \quad (58.34)$$

For the ideal case of a time-mean – strictly – zonal flow (as for a flat bottom) the advection of the time-mean QPV vanishes,  $\mathcal{J}(\bar{\psi}_i, \bar{q}_i) = 0$ , and the divergence of the eddy QPV flux balances locally the curl of the frictional stress, as formulated by (58.5) or (58.17) for momentum. For non-zonal flow, e.g. in the presence of topography, the advection of the time-mean QPV would not vanish in general but the

integral of the mean advection term of areas bounded by time-mean streamlines always vanishes, which implies

$$\oint_{\bar{\psi}_i=\text{constant}} \left( \mathbf{n}_i \cdot \overline{\mathbf{u}'_i q'_i} - \mathbf{t}_i \cdot \bar{\tau}_i / H_i \right) ds = 0, \quad (58.35)$$

where  $\mathbf{n}_i$  and  $\mathbf{t}_i$  are normal and tangential unit vectors with respect to streamlines ( $\bar{\psi}_i$  contours) and  $ds$  is a line element along those contours. An approximate functional relation  $\bar{q}_i \simeq G_i(\bar{\psi}_i)$  is found if the terms on the RHS of (58.34) are small, of the order of a small parameter  $\delta$  that could be the angle between contours of  $\bar{\psi}_i$  and  $\bar{q}_i$ . Such a scenario of a PV balance was suggested by Pierrehumbert and Malguzzi (1984) in a barotropic context. By expanding  $\bar{\psi}_i = \bar{\psi}_i^0 + \delta \bar{\psi}_i^1 + \dots$  with  $\mathcal{J}(\bar{\psi}_i^0, \bar{q}_i^0) = 0$ , where  $\bar{q}_i^0 = G_i(\bar{\psi}_i^0)$ , and assuming a diffusive law for the eddy QPV flux,  $\overline{\mathbf{u}'_i q'_i} = -k_i \nabla \bar{q}_i^0$ , we turn (58.35) into

$$\frac{\partial G_i}{\partial \bar{\psi}_i^0} \oint_{\bar{\psi}_i^0=\text{constant}} k_i \bar{u}_i^{\parallel} ds + \oint_{\bar{\psi}_i^0=\text{constant}} \bar{\tau}_i^{\parallel} ds = 0, \quad (58.36)$$

where  $\parallel$  denotes the component parallel to the  $\bar{\psi}_i^0$  contour. Incidentally, (58.36) is the solvability condition for the first-order equation which determines  $\bar{\psi}_i^1$ . The zeroth-order flow  $\bar{\psi}_i^0$  is, however, determined from (58.31), with the functional  $G_i(\bar{\psi}_i^0)$  introducing the forcing and the effect of the eddy fluxes. As can be seen from (58.36), the problem is of differential-integral type. For the strictly zonal flat-bottom case we recover the simple problem (58.23).

Instead of parameterizing the eddy flux of QPV we may consider parameterization of the functionals  $G_i$ . Then, in contrast to the case of the eddy coefficients, we do not search for functions of position  $y$  but rather for functionals of  $\bar{\psi}_i$  depending on integral properties of the forcing, the parameter of the bottom friction, the channel and layer dimensions, and the parameters which describe the eddy fluxes of QPV. It is clear from the preceding analysis that this task is equivalent to the task of parameterizing the eddy QPV fluxes.

### 58.3 A general transport theory

After discussing simple conceptual models and results from QG numerical models, we turn to a more complete theory resting on experiments with a global numerical model of ocean circulation, namely the Parallel Ocean Program (POP) model, which is based on primitive-equation dynamics and thermodynamics and has eddy resolution (Smith *et al.*, 1992). The aim is a generalized Johnson–Bryden transport theory that includes all relevant terms, in particular the thermodynamic forcing of the zonal current and topographically induced effects.

The POP model is a global model of Bryan–Cox type with an implicit free-surface formulation of the barotropic mode. It uses a Mercator grid, allowing higher resolution

in polar regions (6.5 km at 78°) than in equatorial regions (31.25 km at the equator). The vertical grid varies between 25 m at the surface and 550 m in the deep ocean (altogether there are 20 levels). The surface heat flux is based on Barnier *et al.* (1995). In ocean regions where ice is present, the sea-surface temperature is restored to  $-2^\circ\text{C}$  with a 1-month time scale. The surface salinity is restored to the monthly Levitus climatology (Levitus, 1982). In the high latitudes (poleward of 70°) the temperature and salinity are relaxed to the annual Levitus climatology in the top 2 km. The output used in this study is a 5-year time average, taken from the last of three 10-year simulations using the 1985–1994 European Centre for medium Range Weather Forecasts winds. Each run was initialized from the final state of the previous experiment. A 3-day average of winds was used. Further details of the POP model and experiments are given by Maltrud *et al.* (1998).

The simulated ACC of the POP model is displayed in Fig. 58.8, showing the path of the current by the concentration of sea-surface-height isolines. As in other high-resolution models (e.g. FRAM Group, 1991) and in the observed state of the ocean (from an altimeter, e.g. Le Traon *et al.* [1998], or from sea-surface temperature, e.g. Olbers *et al.* [1992] and Hughes and Ash [2001]), the current is not a single zonal jet but a multiple-fragmented-jet system with a path that is strongly influenced by large-scale topographic features and the gap of Drake Passage, which it has to cross. The gradual southward shifting of the current from the Atlantic throughout the Pacific is in accordance with observations; it is interrupted by the sudden northward excursion in the lee of Drake Passage.

We apply a zonal averaging to the model fields, as done in the previous analysis. Obviously, in a zonally averaged picture many details of such a current system are lost and the single jets will be smeared out. Most importantly, the zonally integrated state in the Drake Passage band of latitudes (about 62°S to 56°S) will not represent the local structure of the current in Drake Passage. Thus, the transport of the averaged current in the Drake Passage band of latitudes is only about 50 Sv whereas the transport in this model through Drake Passage is 130 Sv, which is very close to observations (see Rintoul *et al.* [2001]).

Figure 58.9 displays the basic Eulerian state of circulation of the POP model. The zonal current in the zonally averaged picture still breaks up into clearly identifiable “jets,” of which two are in the Drake Passage belt, a further two are just north of Drake Passage latitudes and must arise from jet features in the Pacific and a moderate eastward turning of the ACC off South America, and two more at about 45°S and 40°S are associated with the confluence zone of the Brazil Current and other jet-like features in the South Atlantic (see Fig. 58.8). The zonal mean potential-density field shows the characteristic features of

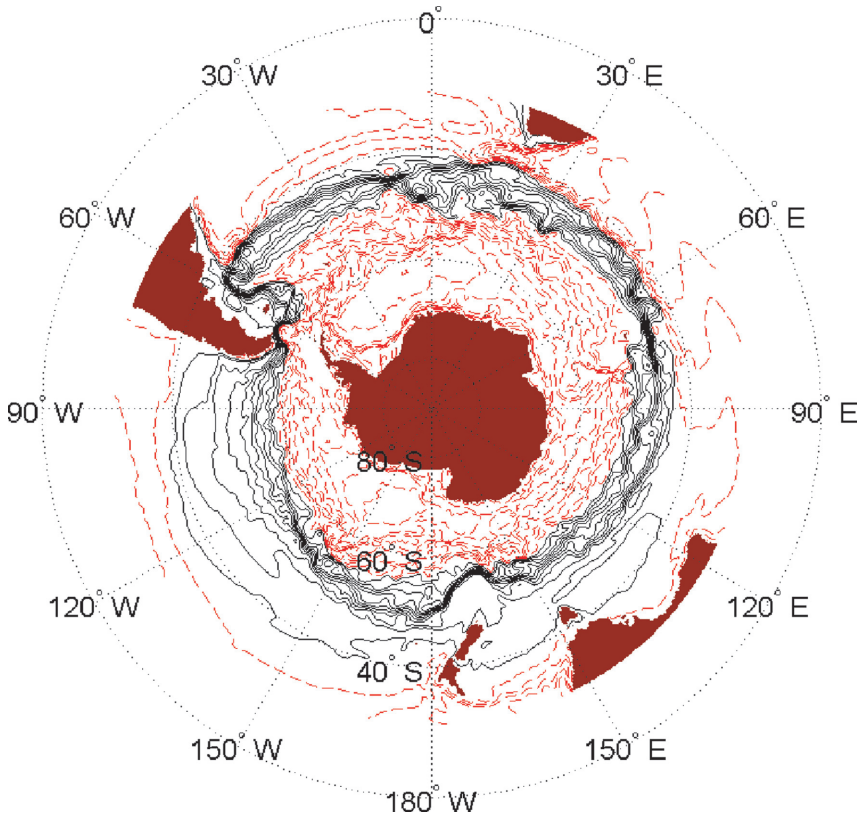


Fig. 58.8. Sea-surface height in the Southern Ocean of POP. Confidence interval 0.1 m. The contours between  $-1.0$  m and  $0$  m are full.

the Southern Ocean stratification: strong gradients in the surface layers (the mixed layer is not resolved), the strong downward slope of isopycnals from the surface to depths of roughly 2000 m, starting at the Drake Passage belt latitudes, and a more or less homogeneous deep layer, extending to the surface in the Antarctic zone (the area south of the Drake Passage belt).

The meridional Eulerian transport, zonally integrated and represented by a streamfunction, is characterized by a fairly strong Deacon cell with a maximum of 27 Sv: the northward transport in the surface layer (the Ekman transport is mostly in the upper two layers, it has a magnitude of roughly 16 Sv in the Drake Passage belt) is returned – in the zonally integrated projection – at great depths, mostly below 2000 m. The structure and dynamics of the Deacon cell are extensively discussed in many studies of the Southern Ocean circulation (Döös and Webb [1994], Karoly *et al.* [1997], see also Rintoul *et al.* [2001]). In the free (unblocked) water column, only ageostrophic meridional transports are possible (which are small because the Reynolds-stress divergence is small), whereas at blocked depths geostrophically balanced transports can appear. In terms of local particle motion the northward flow induced by Ekman dynamics in the surface layer is indeed largely returned at only slightly deeper depths by eddy driving as in QG simula-

tions (the eddy-induced circulation; see below). In terms of zonally integrated mass transport, however, the return transport must occur in the valleys of the blocking topography, or, in cases of small or vanishing topography, by an Ekman bottom boundary flow. In the POP model (and in the real ACC) it occurs by the action of deep southward geostrophic currents. This overturning circulation is the most fundamental difference of this realistic simulation from results of the flat-bottom QG experiments shown above.

Transient eddies result from the ACC jets by instability processes. The POP model resolves the eddy field in a realistic way with reasonable amplitudes (see the kinetic energy of the transient eddies in Fig. 58.9 and the discussion in Best *et al.* [1999]) and thus the mean Eulerian flow is backed by a significant eddy-induced field of transport. In a Lagrangian picture there appears the eddy-induced transport of mass on isopycnals (which is the Stokes-like bolus transport) which, together with residual transport, replaces the Eulerian transport. This concept is outlined in the next section.

### 58.3.1 The transformed-Eulerian-mean framework

Zonal averaging of model equations, as used in the previous analysis, is a basic tool in the interpretation of the dynamics of zonal flow. In the atmospheric application

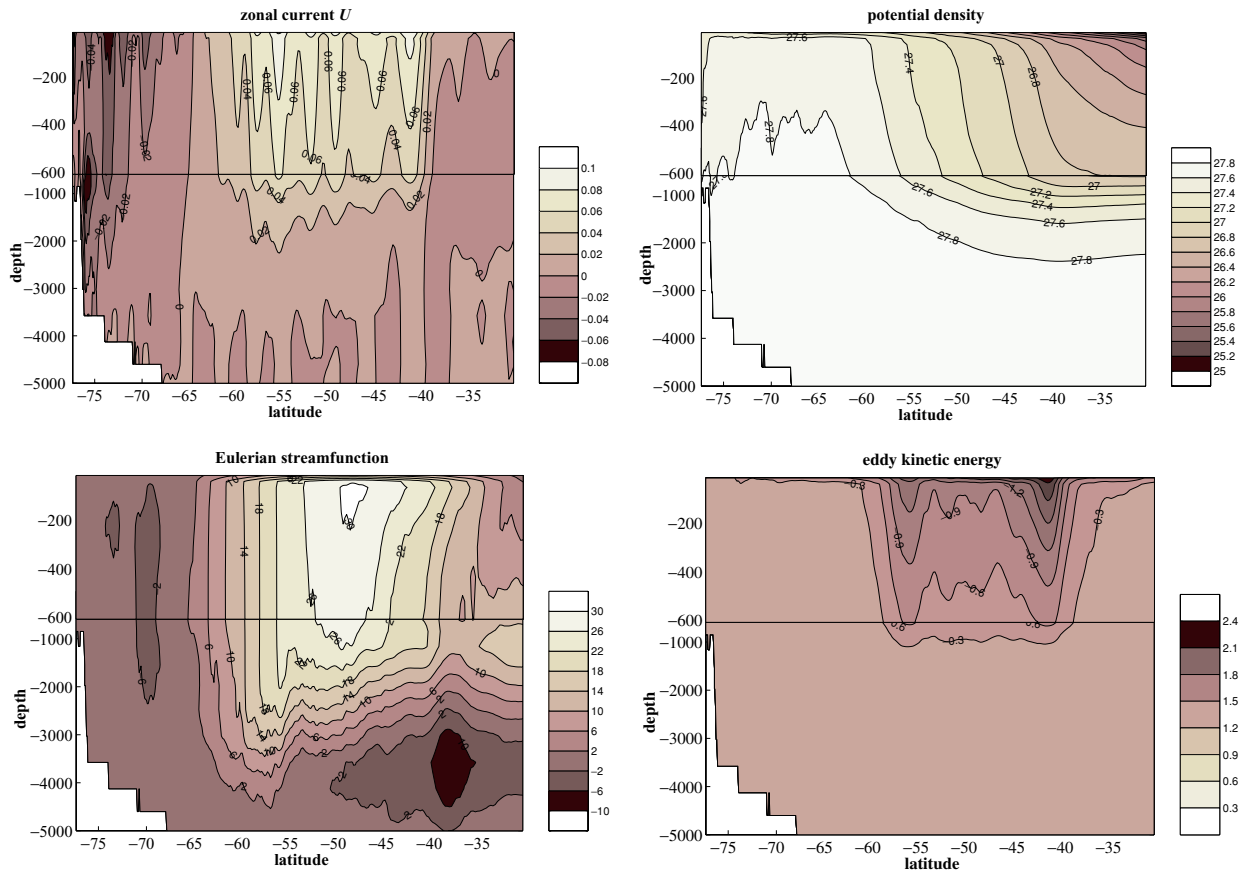


Fig. 58.9. Zonally and time-averaged zonal mean velocity  $U$ , potential-density field  $\Sigma$ , the Eulerian circulation streamfunction  $\phi$ , and the kinetic energy of transient eddies (EKE), as functions of depth and latitude, taken from the POP model. Units are  $U$  in  $\text{m s}^{-1}$ ,  $\phi$  in Sv, and EKE in  $10^{-2} \text{ m}^2 \text{ s}^{-2}$ .

this tool is formalized in the transformed-Eulerian-mean (TEM) framework (e.g. Andrews *et al.*, 1987) and the concept of the residual circulation is frequently invoked. The following derivation of the TEM, which is appropriate for the ocean where topography may block the zonal path, can be found in parts also in McIntosh and McDougall (1996). For more details see also Olbers and Ivchenko (2001). Define time-averaged and zonally integrated<sup>5</sup> variables  $\{\phi\}$  on level surfaces, using the curly-bracket operator, and put  $\phi^* = \phi - \{\phi\}/L$ , with  $L = L(y, z)$  being the length of the circumpolar path at depth  $z$  and latitude<sup>6</sup>  $y$ . The deviation  $\phi^*$  thus contains transient and standing eddies. The balance

<sup>5</sup> These are more convenient than zonally averaged variables in cases of interruption by topography. For example, the zonal integral of a three-dimensional divergence turns into the corresponding two-dimensional divergence of the zonal integral,  $\{\nabla_3 \cdot \mathbf{F}_3\} = \nabla_2 \cdot \{F_2\}$  if the kinematic boundary condition holds for  $\mathbf{F}_3$ .

<sup>6</sup> We simplify equations by use of local Cartesian coordinates. All data evaluations of the POP model are performed in spherical coordinates.

of zonal momentum becomes

$$-f\{v\} = \frac{\partial\{\tau\}}{\partial z} - \frac{\partial}{\partial z}\{uw\} - \frac{\partial}{\partial y}\{uv\} + \sum_{\text{ridges}} \delta\bar{p}_b \quad (58.37)$$

where the overbar is the time average. Lateral subgrid stresses are ignored for simplicity. The sum of the pressure differences  $\delta\bar{p}_b$  is extended over all submarine ridges interrupting the integration path at depth  $z$  (continents are here included). Each ridge or continent contributes the difference between the values on the eastern side and the western side, i.e.  $\delta\bar{p}_b = p(x_E, y, z = -h) - p(x_W, y, z = -h)$ . The interfacial form-stress divergence is introduced into (58.37) by splitting the Eulerian velocity into the eddy-induced – Stokes-like – part and the remaining residual circulation,

$$\{v\} = v_{\text{res}} + \frac{\partial\phi_{\text{ed}}}{\partial z} \quad \{w\} = w_{\text{res}} - \frac{\partial\phi_{\text{ed}}}{\partial y} \quad (58.38)$$

where  $\phi_{\text{ed}} = \{v^*\sigma^*\}/\Sigma_z$  is the eddy-induced streamfunction, with  $\Sigma = \{\sigma\}/L$  the zonal mean of the potential density  $\sigma$  (referred to the surface and normalized by a constant reference density) and  $\{v^*\sigma^*\} = \{v\sigma\} - \{v\}\Sigma$  the eddy flux (transient and standing) of potential density. From mass

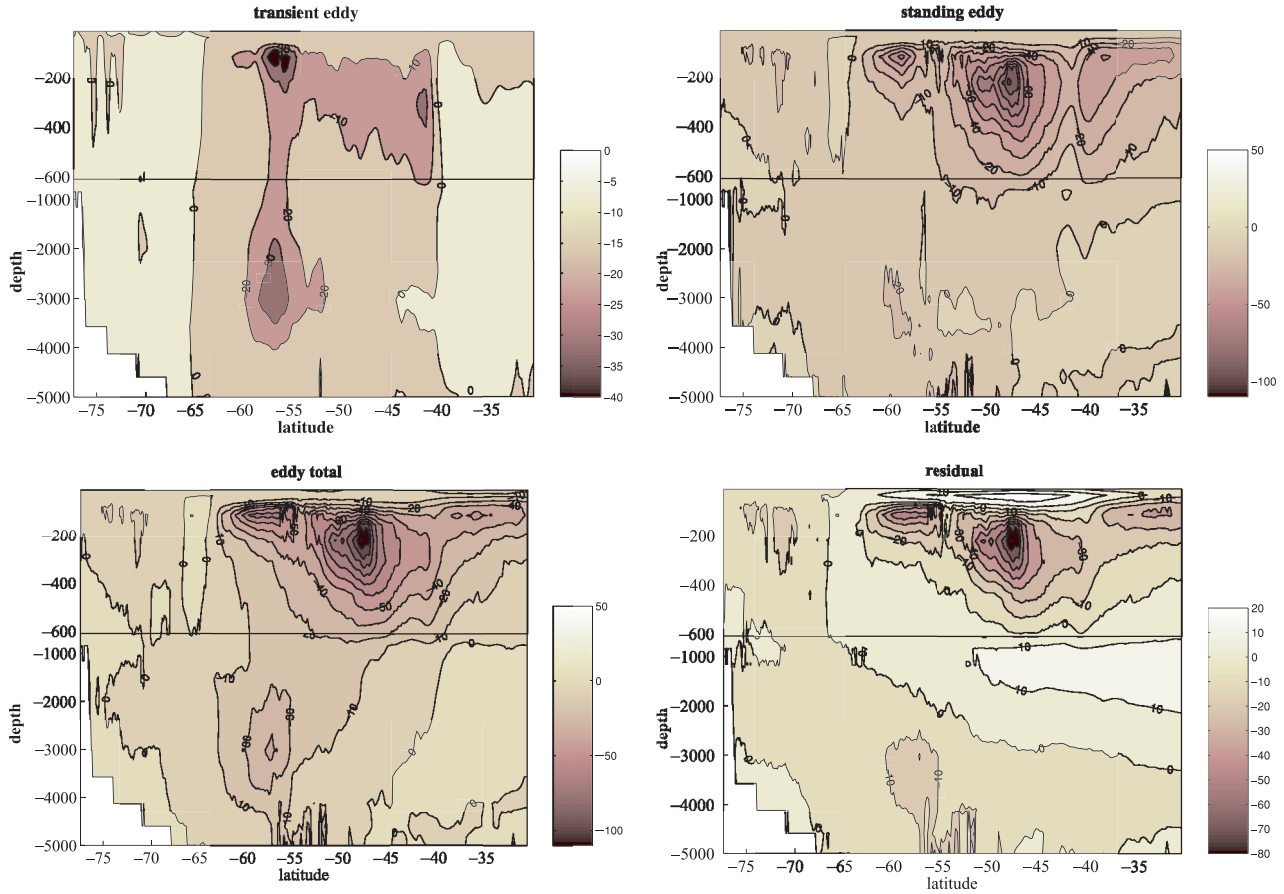


Fig. 58.10. Streamfunctions from the POP model as functions of depth and latitude: transient eddy  $\phi_{\text{trs}}$  (upper-left-hand panel), standing eddy  $\phi_{\text{std}}$  (upper-right-hand panel), eddy total  $\phi_{\text{ed}}$  (lower-left-hand panel), and residual  $\phi_{\text{res}}$  (lower-left-hand panel). Units are Sv. Confidence interval 10 Sv.

balance it can be shown that the vector  $(\{v\} = -\partial\phi/\partial z, \{w\} = \partial\phi/\partial y)$  has a streamfunction  $\phi$  despite possible interruptions of the zonal path by topography. Thus there is a streamfunction  $\phi_{\text{res}} = \phi + \phi_{\text{ed}}$  of the residual circulation as well. We split the advective terms in (58.37) into mean and Reynolds-stress contributions, e.g.  $\{uv\} = \{v\}U + \{u^*v^*\}$  with  $U = \{u\}/L$ , and express the mean terms further by the residual and eddy-induced streamfunctions. In the resulting equation the balance (58.37) appears as residual advection and flux divergences of zonal momentum, driving the zonal mean current  $U$ ,

$$\mathcal{J}(\phi_{\text{res}}, U) + \frac{\partial}{\partial z} (f\phi_{\text{res}} - \{\tau\} + \mathcal{F}) - \nabla \cdot \mathbf{F} = 0, \quad (58.39)$$

where  $\mathcal{J}$  is the  $y, z$ -Jacobian and the Eliassen–Palm vector

$$\mathbf{F} = (-\{u^*v^*\} + \phi_{\text{ed}}U_z, (f - U_y)\phi_{\text{ed}} - \{u^*w^*\}) \quad (58.40)$$

and the bottom form stress  $\mathcal{F}(z)$  for the level interval from hill top down to level  $z$  in the valleys,

$$\mathcal{F}(z) = \int_z^0 \sum_{\text{ridges}} \delta \bar{p}_b \mathbf{d}z = \sum_{\text{ridges}} \int_{x_{\text{W}}(z)}^{x_{\text{E}}(z)} dx \bar{p}_b \frac{\partial h}{\partial x}, \quad (58.41)$$

have been defined. Notice that  $\mathcal{F}(z) \equiv 0$  for levels above the highest topography. For a large-scale flow the Eliassen–Palm vector simplifies to  $\mathbf{F} = (-\{u^*v^*\}, f\phi_{\text{ed}})$ , the divergence of which equals the eddy PV flux (c.f. Eq. (58.5)). In the case of negligible contributions from the Reynolds terms and advection of zonal momentum by the residual circulation, (58.39) describes a balance of momentum that is entirely in terms of vertical fluxes: at each level the interfacial form stress due to the eddy field,  $f\phi_{\text{ed}}$ , is balanced by the flux due to subgrid motion,  $\{\tau\}$ , the flux carried by the residual circulation,  $f\phi_{\text{res}}$ , and the flux due to the bottom pressure gradient,  $\mathcal{F}$ . With these contributions to the momentum balance, the adiabatic flat-bottom regime is generalized to diabatic and topographic conditions.

The eddy and the residual streamfunctions are shown in Fig. 58.10. These look very different from the Eulerian circulation: all have cells with reversed circulations compared with the Deacon cell, and intense cells of significantly smaller sizes are imbedded. The transient eddies induce a narrow, fairly deep-reaching circulation of about  $-10$  Sv in the Drake Passage belt with two imbedded

smaller cells, one in the upper 300 m of the water column (actually a double cell of maximum  $-30$  Sv) and one in the depth range 1500–3500 m (with maximum  $-25$  Sv). A smaller cell appears in the zone of northward deflection of the ACC north of Drake Passage and in the confluence zone further to the north. Standing eddies generate an intensive upper-ocean cell with maximum magnitude  $-80$  Sv in the deflection zone. All these cells add in the total eddy streamfunction which presents a deep-reaching reverse eddy-induced flow of  $-10$  to  $-15$  Sv with imbedded very strong localized cells in the upper ocean and at depth in the Drake Passage belt. In the resulting residual circulation the Deacon cell is replaced by quite a complicated pattern: the three small-scale reversed cells of the transient and standing-eddy contributions appear with fairly strong and compact footprints; they are imbedded in a large-scale weaker flow that is northward in the surface layers (a remnant of the Ekman flow) and southward at great depths (a remnant of the Eulerian geostrophic return flow). Notice that the deep-reaching downward branch of the Deacon cell north of Drake Passage has completely vanished in  $\phi_{\text{res}}$ . The overwhelming importance of standing eddies in the eddy-streamfunction and the residual circulation has been found in other eddy-resolving (or eddy-permitting) models. For FRAM (FRAM Group, 1991) this was shown in Karoly *et al.* (1997).

The residual streamfunction combines mean Eulerian and eddy-induced transports to give the residual transport of potential density in the zonally integrated balance:

$$\mathcal{J}(\phi_{\text{res}}, \Sigma) = -\frac{\partial J}{\partial z}. \quad (58.42)$$

To derive (58.42), the bottom boundary condition on the three-dimensional subgrid flux of  $\sigma$  and the kinematic boundary condition on the three-dimensional velocity are imposed (as described in footnote 5). Notice that eddies affect the zonal mean potential density only via  $J^\perp = (\{v^* \sigma^*\}_{\Sigma_y} / \Sigma_z + \{w^* \sigma^*\})$ , representing the (zonally integrated) eddy flux normal to (zonal-mean) isopycnals. It combines with the diapycnal subgrid flux  $J^d$  for diffusion and convection to give  $J = \{J^d\} + J^\perp$  and enters the balance as a vertical divergence.

We note in passing that other forms of eddy streamfunction have been discussed. If  $J^\perp = 0$  we may obviously write  $\phi_{\text{res}} = -\{w^* \sigma^*\} / \Sigma_y$ , which is the eddy streamfunction of Held and Schneider (1999). It may be used for non-zero  $J^\perp$ , then  $\partial J^\perp / \partial z$  in (58.42) is replaced by  $\partial(-J^\perp / s_\sigma) / \partial y$ , where  $s_\sigma = -\Sigma_y / \Sigma_z$  is the isopycnal slope.

The connection of  $\phi_{\text{res}}$  with subgrid mixing processes and thermohaline surface forcing becomes obvious on regarding the potential density field  $\Sigma(y, z)$  in (58.42)

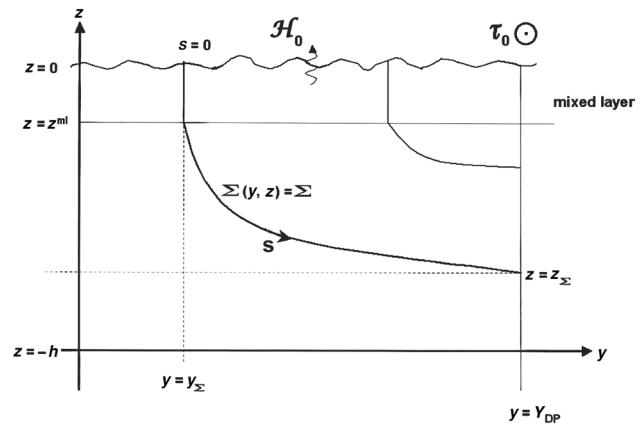


Fig. 58.11. A sketch to show the coordinate system oriented at the isopycnal  $\Sigma(y, z) = \Sigma$ . Antarctica is to the left and  $y = Y_{\text{DP}}$  is in the Drake Passage belt.

as given and solving for the residual streamfunction. The balance (58.42) may be put into the form

$$\frac{\partial \phi_{\text{res}}}{\partial s} = -\frac{1}{|\nabla \Sigma|} \frac{\partial J}{\partial z}, \quad (58.43)$$

where the coordinate  $s$  runs along isopycnals  $\Sigma = \Sigma(y, z) = \text{constant}$  (see Fig. 58.11). Suppose for simplicity that they crop out at the surface ( $s = 0$ ), run through a mixed layer where  $\Sigma = \Sigma^{\text{ml}}(y)$  is vertically constant, and then are subducted into the interior. We may split the solution of (58.43) into a term from the surface flux-boundary condition and one from the interior below the mixed layer, so in the coordinates  $(\Sigma, s)$  we have

$$\phi_{\text{res}}(\Sigma, s) = -\frac{\mathcal{H}_0(\Sigma) - J(\Sigma, z^{\text{ml}})}{|\Sigma_y^{\text{ml}}(\Sigma)|} - \int_{s=z^{\text{ml}}}^s \frac{\partial J / \partial z}{|\nabla \Sigma|} ds', \quad (58.44)$$

where  $(\Sigma, s = 0)$  is the outcrop point of the isopycnal  $\Sigma$  at the surface and  $z = z^{\text{ml}}$  is the depth of the base of the mixed layer at that latitude. The flux at the sea surface,  $\{J^\perp\}(y, s = 0) = \mathcal{H}_0(y)$ , is prescribed as a boundary condition. If  $J^\perp$  vanishes, the residual streamfunction  $\phi_{\text{res}}$  is simply given by subgrid fluxes of density and could strictly be associated with diabatic (thermohaline) physics. Notice, however, that, even if eddies mix only along isopycnals and eddy-induced diapycnal fluxes are zero in a time-mean framework (i.e. the transient-eddy flux vector lies in the time-mean isopycnal), this would not necessarily imply the vanishing of  $J^\perp$ . McIntosh and McDougall (1996), however, showed that the difference between geopotential zonal integration and isopycnal integration is of the order of the cube of the perturbation (eddy) amplitude. Thus, contributions to  $J^\perp$  arising from locally isopycnal transient-eddy flux are of third order whereas contributions from locally diapycnal fluxes are of second order. Hence, in this sense we may associate  $J^\perp$  with diapycnal eddy fluxes and,

consequently,  $\phi_{\text{res}}$  with diabatic processes of water-mass conversion. If eddy mixing is along isopycnals, as is usually assumed in eddy-mixing concepts, we may even neglect  $J^\perp$  altogether.

With  $\phi = 0$  at the surface and solid boundaries to ensure that we have zero normal velocities there, we have also  $\phi_{\text{res}} - \phi_{\text{ed}} = 0$  there and thus (58.39) integrates to

$$-f\phi = f \frac{\{v^* \sigma^*\}}{\Sigma_z} - f\phi_{\text{res}} = \{\tau_0\} - \{\tau\} - \mathcal{R} + \mathcal{F}, \quad (58.45)$$

which is the Johnson–Bryden relation in the most complete form. Here,  $\mathcal{R}(z)$  collects small terms arising from the integral from the top to level  $z$  of the Reynolds stresses, the residual advection of  $U$ , and the  $\phi_{\text{ed}}U$  terms in the Eliassen–Palm vector. Apart from the lateral Reynolds term, the other terms in  $\mathcal{R}$  will be neglected. Upon inserting (58.44) into (58.45), both external forcing functions – wind stress and surface density flux – are implemented in the balance of zonal momentum and the proportion of direct forcing by these agents becomes apparent (for QG dynamics this was derived by Olbers [1993]). Of course, other terms in the balance – the stratification in particular – depend indirectly on the external forcing, but this dependence cannot be revealed easily.

The eddy transport is further split into transient and standing components, setting e.g.  $v^* = \bar{v}^* + v'$ , where the overbar denotes the time average and prime-bearing quantities represent the transient-eddy field. Then

$$\{v^* \sigma^*\} = \overline{\langle v' \sigma' \rangle} + \langle \bar{v}^* \bar{\sigma}^* \rangle \quad (58.46)$$

and correspondingly for the Reynolds stress. The angle brackets denote zonal integration. This implies a separation of the eddy-induced streamfunction into transient and standing contributions,  $\phi_{\text{ed}} = \phi_{\text{trs}} + \phi_{\text{std}}$ . Notice that (58.45) is valid not only at latitudes that are zonally unblocked by continents but also, with the appropriate integration associated with the zonal integration operators  $\{\cdot\cdot\}$  and  $\langle\cdot\cdot\rangle$ , at latitudes that are interrupted by continents.

On taking (58.45) at the maximum depth  $h_m$  along the zonal path, the balance of total zonal momentum is obtained as

$$\{\tau_0\} - \{\tau_b\} + \mathcal{F}(-h_m) - \mathcal{R}(-h_m) = 0, \quad (58.47)$$

where  $\tau_b$  is the frictional bottom stress and  $\mathcal{F}(-h_m)$  is the total bottom form stress. The Reynolds part  $\mathcal{R}$  is generally small, and  $\tau_b$  can be neglected if the bottom topography is sufficiently high. Then, the zonal momentum is balanced by input due to wind stress and removal due to bottom form stress, as assumed in Section 58.1 and demonstrated for the POP model in Fig. 58.12. This proved to be applicable to the POP model as well as to other eddy-resolving

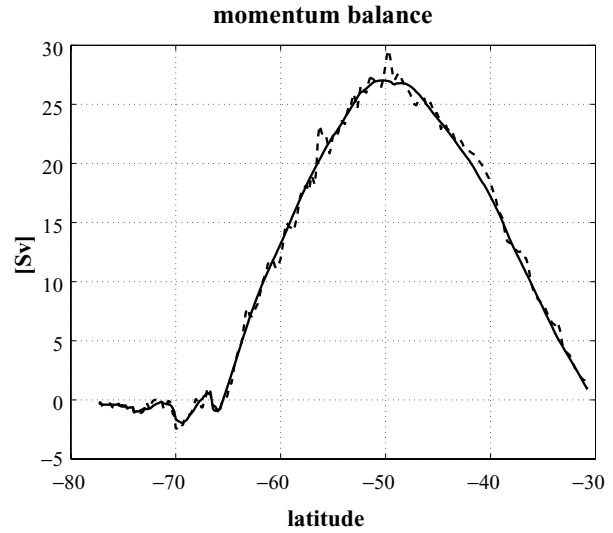


Fig. 58.12. The vertically integrated momentum balance (58.47) (normalized by  $f_0 = 1.25 \times 10^{-4} \text{ s}^{-1}$ ), indicating a balance between wind stress (full) and negative bottom form stress (dashed) at each latitude (small deviations are due to Reynolds-stress effects).

models of the ACC (see e.g. Olbers [1998] and Rintoul *et al.* [2001]).

### 58.3.2 Transport equations

As in Johnson and Bryden (1989), the transient-eddy flux of potential density is parameterized by a down-gradient form,  $\overline{\langle v' \sigma' \rangle} = -\kappa L \Sigma_y$ , and use of the thermal wind relation  $fU_z = g \Sigma_y$  (here we equate density to potential density) then turns (58.45) into a prognostic equation for the shear  $U_z$  of the zonal current. Thus, the parameterization and the balance of momentum imply

$$\kappa L U_z = -\frac{g \Sigma_z}{f} \phi_{\text{trs}}, \quad (58.48)$$

$$f \phi_{\text{trs}} = \{\tau_0\} - \{\tau\} - \mathcal{R} + \mathcal{F} + f(\phi_{\text{res}} - \phi_{\text{std}}). \quad (58.49)$$

Obviously, these equations allow the determination of the zonal current velocity and the associated transport relative to the bottom (or any other reference level) if the diffusivity and the terms on the RHS are known.

In Fig. 58.13 we compare a linear model (i.e. vertically constant  $\kappa$ ) with the non-linear Green–Stone and Visbeck concepts (see Section 58.2.1), using the POP data at latitude 59°S (left-hand panels). The linear model is apparently most appropriate for the POP data below 500 m depth. In the right-hand panel of Fig. 58.13 a vertically constant diffusivity is applied at each latitude. This linear model obviously breaks down south of the Drake Passage belt and in the confluence zone, where negative values of  $\kappa$  result from the fit.

If the terms on the RHS of (58.49) and  $\kappa$  are given, the equations yield by double vertical integration the trans-

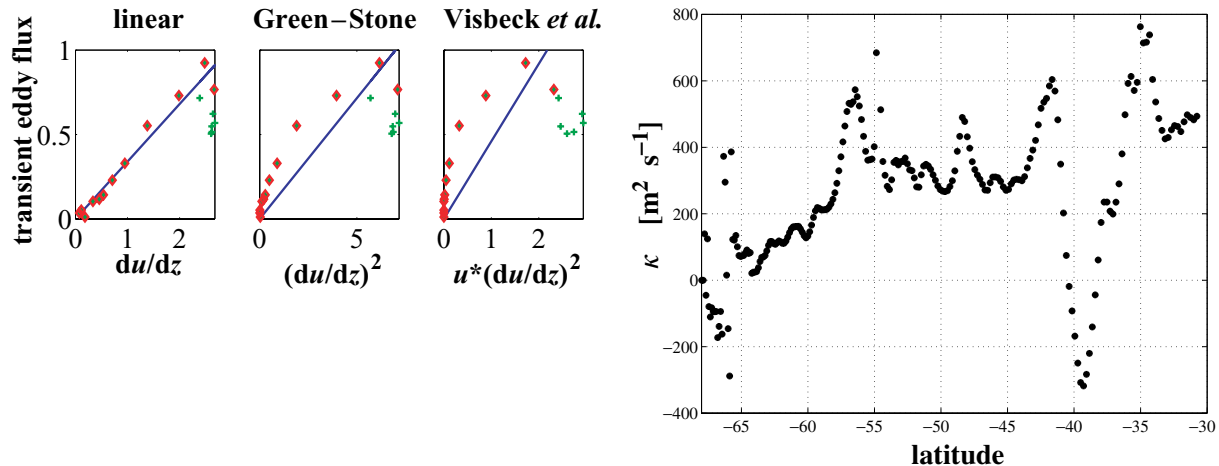


Fig. 58.13. Left-hand panels: three fits to parameterization of the transient-eddy flux of potential density at latitude 59°S (left: linear, middle: Green–Stone, right: Visbeck *et al.*). For the fit, indicated by the straight line, only data below 500 m depth were used (diamonds). The axes are scaled. Right-hand panel: diffusivity  $\kappa(y)$  for the linear fit of the eddy flux to the mean gradient  $\Sigma_y$ . Units are  $\text{m}^2 \text{s}^{-1}$ .

port of the Johnson–Bryden model relative to the bottom,

$$\mathcal{T}_{\text{JB}} - \mathcal{T}_{\text{b}} = -\frac{1}{\kappa} \int_{-h}^0 dz \frac{z}{L} \frac{N^2}{f^2} [(\{\tau_0\} - \{\tau\} - \mathcal{R} + \mathcal{F}) + f(\phi_{\text{res}} - \phi_{\text{std}})], \quad (58.50)$$

where  $\mathcal{T}_{\text{b}} = hU(-h)$  and a local Brunt–Väisälä frequency  $N^2(y, z) = -g\Sigma_z$ . The complete transport of the zonal mean current is thus expressed as a sum of seven terms,

$$\mathcal{T}_{\text{JB}} = \mathcal{T}_{\text{b}} + \mathcal{T}_0 + \mathcal{T}_{\text{fr}} + \mathcal{T}_{\text{R}} + \mathcal{T}_{\text{form}} + \mathcal{T}_{\text{res}} + \mathcal{T}_{\text{std}}. \quad (58.51)$$

Here,  $\mathcal{T}_{\text{fr}}$  represents the contribution from the subgrid stress  $\tau$  in the water column,  $\mathcal{T}_{\text{R}}$  is the Reynolds-stress forcing, and  $\mathcal{T}_{\text{form}}$  results from the bottom form stress. Some of the contributions to the total transport can be expressed more explicitly in terms of the applied external forcings, namely the wind stress and the flux of buoyancy at the sea surface.

The contribution from the Eulerian mean terms deriving from  $\tau_0$  and  $\mathcal{F}$  involves Ekman and geostrophic transports. Here, the abbreviation  $\tau_0 = \{\tau_0\}/L$  is used. They can be expressed as

$$\mathcal{T}_0 = \frac{\tau_0 N_0^2}{\kappa f^2} b^2, \quad \mathcal{T}_{\text{form}} = \frac{1}{2} \frac{N_{\text{b}}^2}{\kappa L f^2} (h^2 - h_{\text{b}}^2) \mathcal{F}(-h). \quad (58.52)$$

The vertical scale  $b$  characterizes the first moment of the local Brunt–Väisälä frequency, such that  $b^2 N_0^2 = -\int z N^2 dz$  and  $b N_0^2 = \int N^2 dz$ , and  $N_{\text{b}}$  refers to some mean value in the deep layer. The parameter  $h_{\text{b}}$  arises from the first moment of the bottom form stress in (58.50); it lies in the interval  $D \leq h_{\text{b}} \leq h$ , where  $D$  is the minimum depth of topographic barriers on the zonal path. The balance of total momentum, Eq. (58.47), may be used to replace the bottom form stress  $\mathcal{F}(-h)$  by  $-L\tau_0$ .

We assume that the subgrid stress  $\tau$  is effective only in Ekman layers of thickness  $\delta$  close to the surface and

bottom. Then, assuming a linear decrease of the stress in these layers, we obtain

$$\mathcal{T}_{\text{fr}} \approx \frac{\tau_{\text{fr}} N_{\text{fr}}^2}{\kappa f^2} \delta^2, \quad (58.53)$$

where the index fr refers either to the frictional surface or to the bottom layer. Thus,  $\mathcal{T}_{\text{fr}}$  is very small relative to  $\mathcal{T}_0$ , of order  $(\delta/b)^2$ , and, even if the bottom is flat and the wind stress must be balanced by the frictional stress at the bottom, i.e.  $\tau_{\text{fr}} \approx \tau_0$ , the frictionally induced zonal transport  $\mathcal{T}_{\text{fr}}$  is negligible.

The contribution from  $\phi_{\text{res}}$ ,

$$\mathcal{T}_{\text{res}} = -\frac{1}{\kappa f} \int_{-h}^0 dz \frac{z N^2}{L} \phi_{\text{res}}, \quad (58.54)$$

describes the thermohaline forcing of the zonal mean current. We consider the solution (58.44) of  $\phi_{\text{res}}$  in terms of the surface-flux and interior-conversion terms. Suppose now for simplicity that all isopycnals crossing the latitude  $y = Y_{\text{DP}}$  of Drake Passage – where (58.54) is considered – outcrop to the south (see Fig. 58.11 for a schematic view and Fig. 58.9 for the POP model) so that the condition  $\Sigma(Y_{\text{DP}}, z) = \Sigma^{\text{ml}}(y = y_{\Sigma})$  maps the depth interval at  $Y_{\text{DP}}$  on to the latitude band south of Drake Passage, resulting in  $y = y_{\Sigma}(Y_{\text{DP}}, z)$  or  $z = z_{\Sigma}(Y_{\text{DP}}, y)$ . If we insert (58.44) into (58.54), two contributions to the ACC transport arise from thermohaline fluxes in the system, one from fluxes across the sea surface south of Drake Passage and one from fluxes across the zonal mean isopycnals in the interior, also south of Drake Passage.

In the following analysis, the above analytical forms for  $\mathcal{T}_0$ ,  $\mathcal{T}_{\text{fr}}$ , and  $\mathcal{T}_{\text{form}}$  are not used; instead, they are evaluated from the POP data directly. All transport terms in (58.51) are functions of latitude and the volume

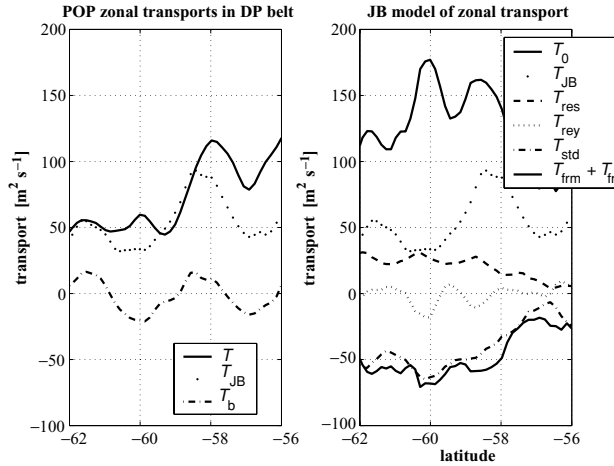


Fig. 58.14. Left-hand panel: mean zonal transport in the Drake Passage belt. Right-hand panel: estimates of various transport terms in the separation (58.51).

transport of the zonal mean ACC is then obtained by integration across the Drake Passage latitudes. Figure 58.14 shows the  $\mathcal{T}$  terms obtained from POP data. Here,  $\mathcal{T}$  and  $\mathcal{T}_b$  use the simulated profile  $U(z)$  of the zonal mean current. The left-hand panel also shows the transport  $\mathcal{T}_{JB}$  of the Johnson–Bryden model. It is revealed here that the constant- $\kappa$  fitting procedure, using only data from below 500 m, is incapable of reproducing the upper-level fluxes (see Fig. 58.13), leading to a discrepancy between  $\mathcal{T}$  and  $\mathcal{T}_{JB}$ . The other  $\mathcal{T}$  terms are obtained using the above expression (58.50) and data from the POP model’s output. They are displayed in the right-hand panel of Fig. 58.14.

A few outstanding signatures are readily extracted from Fig. 58.14. It is obvious that the part of transport relative to the bottom,  $\mathcal{T} - \mathcal{T}_b$ , carries most of the transport: although the bottom transport is locally a 20% contribution, its alternating sign yields a very low value in the integral. With respect to forcing mechanisms the direct wind forcing ( $\mathcal{T}_0$ ) is clearly dominant. Together with the thermohaline forcing ( $\mathcal{T}_{res}$ ) it establishes eastward flow. Retarding mechanisms, yielding westward transports, are the bottom form-stress component  $\mathcal{T}_{form}$  and the standing eddies  $\mathcal{T}_{std}$ , the first slightly leading in magnitude. The Reynolds stress forcing is of alternating sign and is insignificant.

### 58.3.3 Scaling theory

Scaling may be applied to extend limited knowledge from limited numerical experiments. We investigate the extended Johnson–Bryden model from Section 58.3 in a broader context. The stratification is represented by a buoyancy jump  $\Delta B = -g\Delta\Sigma$ , occurring over a depth scale  $d$  in the vertical and over  $Y$  in the meridional direction (the latter scale is assumed given). Neglecting subgrid and Reynolds stresses (which are small) and the standing-eddy

term (which is not small but beyond parametrical treatment), the zonal balance is expressed as<sup>7</sup>

$$\kappa U_z = \frac{\Delta B}{df^2} \left( \tau_0 + \frac{f}{L} \phi_{res} \right). \quad (58.55)$$

The effect of bottom form stress shielding part of the wind stress according to (58.52) is assumed to be included in the wind-stress term. The residual streamfunction is related to the density flux  $\mathcal{H}_0$  by  $\phi_{res} \Delta B / (LY) \sim \mathcal{Q}_0 = -g\mathcal{H}_0/L$ , using the density balance in the integrated form (58.44). The zonal balance must be consistent with the meridional balance, or, in terms of the thermal wind relation, with  $U_z = \Delta B / (fY) = U/d$ . Hence, we arrive at

$$\kappa \frac{d}{Y} \sim \frac{\tau_0}{f} + \frac{\mathcal{Q}_0}{\Delta B/Y} \quad (58.56)$$

with the zonal mean buoyancy flux  $\mathcal{Q}_0$ . This equation relates the slope of the isopycnals to the forcing and eddy effects appearing here in terms of the diffusivity  $\kappa$ . Remember that  $\tau_0$  is a measure of the zonal mean wind stress in the Drake Passage belt whereas  $\mathcal{Q}_0$ , according to (58.44), is collected from the isopycnal outcrops in the Antarctic zone.

A Green–Stone parameterization (see Section 58.2.1) has  $\kappa = \alpha f \ell^2 / \sqrt{\mathcal{R}_i}$ , with  $\ell = \pi^2 \lambda$  proportional to the internal Rossby radius  $\lambda = Nd / (f\pi)$  (which is based on  $d$ ). The diffusivity becomes  $\kappa = \alpha \pi^2 (d \Delta B)^{3/2} / (f^2 Y)$  and the balance (58.56) may be written as

$$\gamma U^{5/2} \sim \frac{U}{d} \tau_0 + \mathcal{Q}_0 \quad (58.57)$$

with  $\gamma = \alpha \pi^2 / \sqrt{Yf}$ . Without additional assumptions this relation yields for weak wind stress<sup>8</sup>  $\gamma U^{5/2} \sim \mathcal{Q}_0 / f$ . In this regime  $U$  would thus be a weak function of the buoyancy flux. For strong wind we obtain  $\gamma d U^{3/2} \sim \tau_0 / f$ , which, however, does not completely remove all internal scales since  $d = d(\tau_0, \mathcal{Q}_0, \dots)$ . This also happens to the transport  $\mathcal{T} = dU$ . The magnitude of the observed wind field places the interest more on the limiting case of strong winds.

The lesson from this scaling attempt is that the zonally averaged equations are insufficient to gain a complete scaling theory. Both momentum balances and the buoyancy balance have been used to determine the dependences of the four unknown quantities  $U_z$ ,  $\phi_{res}$ ,  $\Delta B$ , and  $d$  on the forcing parameters  $\tau_0$  and  $\mathcal{Q}_0$ . An additional phenomenological relation must be found from numerical modeling or physical reasoning.

<sup>7</sup>  $f$  is the modulus of the Coriolis parameter in the following.

<sup>8</sup> With  $\mathcal{Q}_0 = 5 \times 10^{-9} \text{ m}^2 \text{ s}^{-3}$ ,  $Y = 2000 \text{ km}$ , and  $\Delta B = 5 \times 10^{-3} \text{ m s}^{-2}$ , weak wind stress is  $\tau_0 \ll 2 \times 10^{-4} \text{ m}^2 \text{ s}^{-2}$ .